Max-Planck-Institut
für Meteorologie

REPORT No. 143

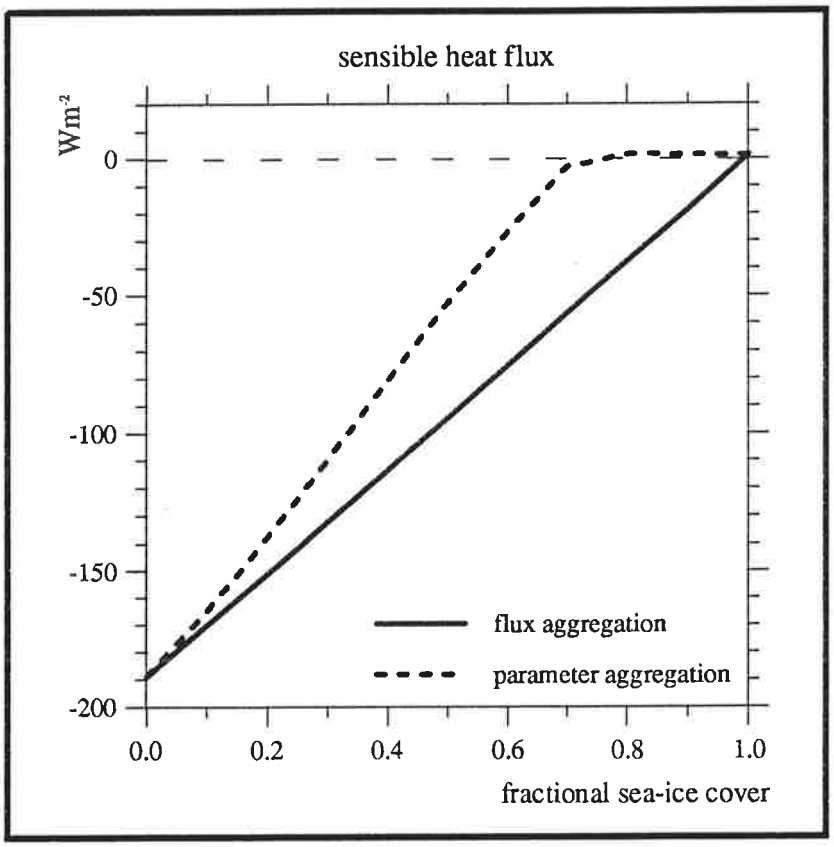

THE IMPACT OF SUB-GRID SCALE SEA-ICE INHOMOGENEITIES ON THE PERFORMANCE OF THE ATMOSPHERIC GENERAL CIRCULATION MODEL ECHAM

by

ANSELM GRÖTZNER · ROBERT SAUSEN · MARTIN CLAUSSEN

HAMBURG, September 1994

AUTHORS:

Anselm Grötzner

Meteorologisches Institut
der Universität Hamburg
Bundesstraße 55
D-20146 Hamburg
FRG

Robert Sausen

Deutsche Forschungsanstalt
für Luft- und Raumfahrt (DLR)
Institut für Physik der Atmosphäre
Oberpfaffenhofen
D-82234 Weßling
FRG

Martin Claussen

Max-Planck-Institut
für Meteorologie

MAX-PLANCK-INSTITUT
FÜR METEOROLOGIE
BUNDESSTRASSE 55
D-20146 Hamburg
F.R. GERMANY

Tel.: +49-(0)40-4 11 73-0
Telefax: +49-(0)40-4 11 73-298
E-Mail: <name>@ dkrz.d400.de

The impact of sub-grid scale sea-ice inhomogeneities on the performance of the atmospheric general circulation model ECHAM

Anselm Grötzner[1], Robert Sausen[2] and Martin Claussen[3]

[1] Meteorologisches Institut der Universität Hamburg, Bundesstraße 55, 20146 Hamburg, Germany
[2] Institut für Physik der Atmosphäre, DLR, Oberpfaffenhofen, 82234 Weßling, Germany
[3] Max-Planck-Institut für Meteorologie, Bundesstraße 55, 20146 Hamburg, Germany

Abstract

Leads and polynyas have a great impact on the energy budget of the polar ocean and atmosphere. Since atmospheric general circulation models are not able to resolve the spatial scales of these inhomogeneities, it is necessary to include the effect of fractional sub-grid scale sea-ice inhomogeneities on the climate by a suitable parameterization.

In order to do this we have divided each model grid-cell into an ice-covered and an ice-free part. Nevertheless, a numerical model requires effective transports representative for the whole grid-box. A simple procedure would be to use grid averages of the surface parameters for the calculation of the surface fluxes. However, as the surface fluxes are nonlinear dependent on the surface properties, the fluxes over ice and open water should be calculated separately according to the individual surface-layer structure of each surface type. Then these local fluxes should be averaged to obtain representative fluxes.

Sensitivity experiments with the Hamburg climate model ECHAM clearly show that a sub-grid scale distribution of sea ice is a dominant factor controlling the exchange processes between ocean and atmosphere in the Arctic. The heat and water vapour transports are strongly enhanced leading to a significant warming and moistening of the polar troposphere. This affects the atmospheric circulation in high and mid-latitudes; e.g the stationary lows are modified and the transient cyclonic activity over the subpolar oceans is reduced remarkably.

A pronounced impact of sub-grid scale sea-ice distribution on the model climate can only be obtained when the nonlinear behaviour of the surface exchange processes is considered by a proper, physically based averaging of the surface fluxes. A simple linear averaging of surface parameters is not sufficient.

ISSN 0937–1060

1. Introduction

The climate system consists of the atmosphere, the hydrosphere (oceans, lakes and rivers), the land surfaces, the cryosphere (snow, ice shields and sea ice), and the biosphere. The sea ice as a part of the cryosphere plays an important role in the earth's climate due to its physical properties and essential influence on the coupling of ocean and atmosphere.

The climate system is affected by the sea ice in several ways. Due to its high albedo, sea ice reduces the fraction of the solar radiation absorbed at the surface of the earth. As the thermal conductivity of ice is relatively low, it isolates the ocean from the atmosphere. If sea ice is present, the temperature at the lower boundary of the atmosphere changes from the sea-surface temperature, which is always higher than -1.9° C, to the ice or snow surface temperature, which can drop below -30° C in winter. Thus, the presence of sea ice drastically modifies the thermal radiation budget. Furtheron, the compact ice cover acts as an effective obstacle for the turbulent exchanges of sensible heat, water vapour and other gases. Finally, the exchange of momentum between ocean and atmosphere is also affected by the sea ice.

Because of these important physical aspects, it is necessary to include sea-ice properly in numerical climate models. In atmospheric general circulation models (AGCMs), sea ice is usually prescribed as a fixed lower boundary condition according to an "observed" climatological sea-ice coverage (e.g. Alexander and Mobley, 1976). A rather simple method is to deduce the sea-ice cover from observed sea-surface temperatures (SST) and to increase the albedo for those regions where the SST drops below the freezing point of sea water (ECMWF, 1991). More sophisticated models assume a prescribed extent and thickness of the sea ice (e.g from observations) and calculate the ice-surface temperature from a heat balance equation (Roeckner, 1992).

In oceanic general circulation models the sea ice is more often treated as an interactive part of the climate system. This is generally the case for global coupled atmosphere-ocean models. Usually, growth and decay of sea-ice are simulated by a thermodynamic sea-ice model (e.g. Washington et al., 1976; Maier-Reimer et al., 1993). In highly sophisticated models, the sea-ice dynamics is also included by considering transport and mechanical deformation of the ice according to the rheology of viscous-plastic media (Hibler, 1986; Oberhuber, 1993). Various investigations showed that in high and mid-latitudes the results of global climate simulations with such models are highly dependent on the treatment of the sea-ice component (e.g.. Meehl and Washington, 1990; Manabe et al., 1992). Especially in coupled atmosphere-ocean models, areas covered with sea-ice seem to be very substantial for the results of the simulations (Schlesinger and Mitchell, 1985). Sea ice appears to be responsible for longtime variability on time-scales of decades with high amplitudes (Cubasch et al., 1992; Lunkeit, 1993; Lunkeit et al., 1994). Therefore, the proper representation of sea

ice is a great challenge for the development of climate models.

The physical representation of sea ice is complicated by the fact that it is not a homogeneous medium. Sea ice is deformed by various forces (e.g. wind stress, ocean currents) and the ice cover is often intersected by areas of open water called leads and polynyas (Smith et al., 1990). The fractional ice cover can vary in a wide range from a few percent near the ice edge up to a very dense ice cover, e.g. in the inner Arctic Ocean. These areas of open water reveal considerable differences to the sea ice in their aerodynamic, thermal and radiative properties. The temperature of an ice layer adjusts rapidly to that of the overlying air due to the low thermal conductivity of the ice. Therefore, the vertical temperature differences and consequently the turbulent fluxes of sensible and latent heat from the air to the ice surface and vice versa are small. Patches of open water break the continuity of the insulating ice. The heat exchange between water and air becomes very intense. Particularly in winter when the surface temperature difference between open water and near surface temperature can be 40 K. Hence one might expect that the surface heat fluxes from the leads have a great influence on the development of the climate of the polar regions (e.g. Ledley, 1988).

Most of the inhomogeneities of the sea ice have spatial scales that cannot be resolved by present global circulation models, which allow only a rather coarse horizontal resolution. Therefore, most GCMs treat sea ice as a continuum. It is assumed that a surface grid box is either totally covered by ice or totally free of ice. As mentioned before, small scale areas of open water in the sea ice (leads) have a great impact on the air-sea exchange processes. Therefore, the leads should be included by a proper parameterization.

A straight forward procedure would be to divide each grid cell in an ice-covered and an ice-free part according to the relative sea-ice compactness. Then effective surface parameters (e.g. temperature, roughness, albedo) could be calculated as weighted averages of the individual local surface parameters of the ice and open water, respectively. These effective parameters are assumed to be valid for the whole model grid-cell and are used to calculate the effective air-sea fluxes for each grid cell. Such a procedure has been applied by Lunkeit et al. (1994) in a longtime integration with a coupled ocean-atmosphere model.

However, the surface fluxes of mass, energy, and momentum are nonlinear dependent on the surface characteristics and the structure of the overlying atmospheric boundary layer. The sensible heat flux to the atmosphere arising from even small leads can be very large due to the strong turbulence under unstable stratified conditions. Sensible heat fluxes of several hundreds of watts per squaremeter (Smith et al., 1990) have been observed. These upward fluxes sometimes dominate the transports of large areas of otherwise stable stratification over the ice. Thus, the averaged stratification of a larger area can be stable whereas the resulting transport is upwards directed, "counter" to the averaged temperature gradient. This process

is quite important in winterly polar ice zones (e.g.. Stössel and Claussen, 1993).

Moreover, the surface parameters and the heat fluxes over ice and water are governed by different physical processes. For instance, the surface temperature of the ice is influenced by the heat conduction into the ice whereas the temperature of the sea water is determined by the enormous heat capacity of the water and horizontal and vertical transports in the ocean. Therefore, the estimation of effective parameters by weighted averaging of the local properties is quite problematic. In order to avoid these problems arising from effective parameters, we suggest to calculate the fluxes for ice-covered and ice-free regions separately and to determine the weighted average of these fluxes. These averages are assumed to be valid for the whole grid-cell and are consecutively transferred to the atmosphere. This method is related to the so-called blending-height concept, which as been successfully applied in the microscale and mesoscale (Claussen 1991a, 1994b). Such a procedure has been also included into a global circulation model by Meleshko et al. (1990) but not examined in detail. Simmonds and Budd (1991) applied a similar method in an AGCM in order to study the impact of a rather crude lead distribution on the Southern Hemispheric winter circulation. They found significant anomalies of the surface fluxes and the state of the atmosphere connected with the sea-ice modifications. Stössel and Claussen (1993) applied the blending-height concept to the atmospheric forcing of a sea-ice model of the Southern Hemispheric Ocean and achieved substantial improvements concerning sea-ice thickness and drift velocities.

In the following we describe different methods for including sub-grid scale sea-ice inhomogeneities into a GCM (Section 3). We implemented these approaches into the Hamburg climate model ECHAM, which is described in Section 2. The impact on the model climate is studied by means of numerical simulations. In Section 4 we present the experimental design to test the parameterizations. Then (Section 5) we will discuss the impact of the different parameterizations of sub-grid scale sea-ice distribution on the Northern Hemispheric winter circulation. A summary and outlook (Section 6) will conclude our paper.

2. The atmospheric general circulation model

The model used for the experiments presented in this paper is the global atmospheric general circulation model ECHAM3 (Roeckner et al., 1992). The prognostic variables are vorticity, divergence, temperature, the logarithm of the surface pressure, and the mixing ratios of water vapour and cloud water, respectively. The model equations are solved on nineteen vertical levels in a hybrid pressure-sigma coordinate system by using the spectral transform method with triangular truncation at total wavenumber n=21 (T21). In general, the model is also

applied with spectral resolutions of T42, T63, and T106. Nevertheless, for the sensitivity studies presented in this paper, the coarse resolution version was thought to be sufficient to demonstrate the impact of the various parameterizations. A higher resolution would result only in quantitative differences. Non-linear terms and physical processes are evaluated at grid-points of a "Gaussian grid" providing a nominal resolution of approx. 5.6° in latitude and longitude. A second order horizontal diffusion scheme is applied beyond a threshold wavenumber n=15 with varying diffusion coefficients for different variables and levels.

The model physics contains all the processes necessary for climate sensitivity experiments. The radiation scheme uses a broad-band formulation of the radiative transfer with six spectral intervals in the terrestrial infrared and four intervals in the solar part of the spectrum. Gaseous absorption due to water vapour, carbon dioxide and ozone is taken into account as well as scattering and absorption due to aerosols and clouds. The cloud optical properties are parameterized in terms of the simulated cloud water content. In general, the surface albedo is a fixed function of longitude and latitude but depends on the declination of the solar radiation. For sea-ice and snow-covered areas, the albedo is also dependent on the temperature of the ice and snow, respectively.

The convection scheme comprises the effects of deep, shallow, and mid-level convection on the budgets of heat, water vapour, and momentum. Cumulus clouds are represented by a bulk model including the effect of entrainment and detrainment on the updraft and downdraft convective mass fluxes. Stratiform clouds are calculated through a cloud water budget equation (ice and liquid phase) including sources and sinks due to condensation, evaporation, and precipitation formation by coalescence of cloud droplets and sedimentation of ice crystals. Sub-grid scale condensation and cloud formation is taken into account by specifying appropriate thresholds for the relative humidity depending on height and stability.

The soil model comprises the budgets of heat and water in the soil, the snow pack over land, and the heat budget of permanent land ice. The heat transfer equation is solved in a five-layer model assuming vanishing heat flux at the bottom, which is located at a depth of 10 m. Vegetation effects such as interception of rain and snow in the canopy, and the stomatal control of evapotranspiration are parameterized in a highly idealized way. The runoff-scheme is based on catchment considerations and takes into account sub-grid scale variations of field capacity over inhomogeneous terrain. The top surface temperature of sea ice is calculated by a simple energy balance equation assuming a constant ice thickness of 2 m in the Arctic and 1 m around Antarctica. The thickness is a crucial factor of the energetics of the sea ice (Maykut, 1978). However, as we intended to analyse the influence of leads as patches of open water, the sea-ice thickness has been kept constant at its operational value.

The turbulent transfer of momentum, heat, water vapour, and cloud water is based on an

eddy diffusivity approach above the atmospheric surface layer. The eddy diffusion coefficients depend on wind shear, mixing length, and Richardson number. The parameterization of the turbulent fluxes of momentum, heat, and water vapour in the surface layer, which are important in the context of this paper, is based upon the Monin-Obukhov similarity theory of the following form:

$$-\overline{(w\psi)}_G = C_k(Ri,z_0)\ (\ \Psi_{19} - \Psi_G\ ) \qquad (1)$$

where Ψ represents the grid box average of the respective quantity that is transported by the turbulent fluxes, e.g. the mean of the horizontal velocity components U and V, the mean of the potential temperature Θ, or the mean of the specific humidity Q. ψ symbolizes the deviation from the mean Ψ, i.e. fluctuating or turbulent part. Ψ_{19} represents the values at the lowest model layer, which is regarded as the atmospheric surface layer, while Ψ_G refers to values at the ground. w is the turbulent vertical velocity, and C_k is a bulk transfer coefficient ($k=m$ for momentum, $k=h$ for sensible and latent heat). The determination of the transfer coefficient is based on the Monin-Obukhov similarity theory, using the Richardson number Ri of the lowest atmospheric layer and a local roughness length z_0.

The application of such a parameterization scheme assumes that the surface layer flow can be treated as a steady state, horizontally homogeneous flow that is in equilibrium with the underlying surface. However, except over vast regions of horizontally homogeneous surface conditions, such as over some portions of the oceans, the atmospheric boundary layer is rarely an equilibrium flow. Rather it has always to adjust to changing surface conditions. However, for variations of sufficiently large scale, the surface layer is commonly supposed to be in local equilibrium with the lower boundary. This assumption justifies the use of conveniently simple parameterization schemes based on boundary-layer similarity theory. With surface inhomogeneities at smaller scales, particularly at scales smaller than resolved by the grid, e.g. the sub-grid scale sea-ice distribution, these practical parameterization schemes are no longer applicable. In this case the problem of properly estimating grid averages of the surface fluxes of heat and momentum and of the spatially varying surface-layer flow arises.

The model ECHAM3 rather realistically reproduces observations. A basic climatology is given in Roeckner et al. (1992). Various versions of the model have already been applied successfully for climate sensitivity studies (e.g. Claussen and Esch, 1993; Graf et al., 1993; König et al., 1993; Ponater et al., 1994) or as atmospheric part of global warming simulations (e.g. Cubasch et al., 1992; Lunkeit et al., 1994).

3. Calculation of surface fluxes above sea ice with sub-grid scale inhomogeneities

Traditionally, the sea-ice cover used in GCMs is derived from observations of the sea-surface temperature (e.g. ECMWF, 1991). Below a certain threshold (i.e. the freezing point of sea water) the ocean is set to be totally ice covered and vice versa. A more direct method derives the ice distribution from ice charts supplied by weather services. Today, satellite observations (e.g. Martin, 1993) of sea ice are available which directly contain the fractional ice cover of the ocean at a given image pixel. A certain threshold, e.g. 50% fractional ice cover, could also be applied for dividing the sea surface of the model in either ice-covered or ice-free gridpoints (Alexander and Mobley, 1976). A threshold of 50 % would be optimal for processes that are linearly dependent on the surface properties, like solar radiation on the surface albedo. Values different from 50 % would be better for non-linear processes like the turbulent transports. But since we have to consider several processes with different characteristics such an optimization seems to be impossible.

A straight forward procedure to parameterize the sub-grid scale ice distribution would be to divide each model grid cell in an ice-covered and an ice-free part according to the observations of the relative sea-ice cover. Effective surface parameters could be calculated by a weighted average of the individual local properties of each fraction. The mean values are then assumed to be valid for the whole grid cell and are used to calculate the total vertical transports. Such a procedure is called "parameter-aggregation" (Claussen, 1994a, 1994b).

Wood and Mason (1991), Noilhan and Lacarrère (1992) have proposed to apply the method of parameter aggregation to the estimation of areally averaged heat fluxes in the case of stratified flow, i.e. by defining proper values of aggregated albedo, surface temperature, ground heat capacity or soil wetness. Lunkeit et al. (1994) applied a similar procedure when they determined the effective surface temperature over sea ice in their coupled model by a non-linear averaging according to the Stefan-Boltzman law for long-wave radiation. However, as we mentioned before, some other exchange processes are non-linearily dependent on the surface parameters in different ways. Moreover, the surface conditions of ice and water are determined by totally different physical processes. Thus, parameter aggregation will fail, because these complications make the definition of aggregated parameters impossible.

In order to circumvent these problems, it has been suggested to compute momentum and heat fluxes for each surface type separately (e.g. Claussen, 1991a). Consecutively, the averaged surface fluxes are obtained by the average of the surface fluxes of each surface type weighted by its fractional area f_k. These weighted averages are assumed to represent the larger scale

properties of each grid cell. This method is called "flux aggregation" (Claussen, 1994b). It is the most physically based method for inclusion of sub-grid scale sea-ice inhomogeneities into a GCM, because it takes into account the local conditions over sea ice and open water and calculates effective transports under consideration of the non-linearities of the surface fluxes.

For the parameterization of areally averaged turbulent fluxes over heterogeneous terrain, the so-called "blending-height concept" has become a useful approach (Mason, 1988; Claussen, 1991a, 1991b). When air flows over a heterogeneous surface, the boundary layer cannot longer be treated to be in a steady state and horizontally homogeneous. The flow has to adjust to the varying surface characteristics, and internal boundary layers develop. The surface exchange processes inside of those internal boundary layers depend on local properties of the surface and the overlying air. Further away from the surface, these internal boundary layers merge, and the individual differences of the surfaces are no longer visible. The blending-height concept is based on the assumption that the flow can be assumed to be independent from horizontal position above a certain height. Therefore it has been suggested (Wieringa, 1986) to average local fluxes at the blending height in order to obtain fluxes representative for larger areas. Mason (1988) defines the blending height l_b as the scale height where the flow changes from equilibrium with the local surface to independence of horizontal position. Above the blending height, modifications of air flow due to changes in surface conditions will not be recognizable individually, but an overall stress or energy flux profile will exist, representing the surface conditions of a large area.

Using this definition, the momentum flux $[-\overline{uw}]$ on average over a heterogeneous surface under neutral conditions is

$$[-(\overline{uw})] = \sum_k -(\overline{uw})_k \cdot f_k = \kappa^2 \, U^2(l_b) \sum_k \frac{f_k}{(\ln \frac{l_b}{z_0^k})^2} \qquad (2)$$

where [...] denotes a horizontal average, f_k is the fractional area covered by a surface type "k" with the roughness lengths z_0^k. U is the mean wind speed taken at the blending height, and κ is the von Kármán constant. From this equation also an aggregated roughness length z_{0a} can be defined by:

$$\frac{1}{(\ln \frac{l_b}{z_{0a}})^2} \equiv \sum_k \frac{f_k}{(\ln \frac{l_b}{z_0^k})^2} \qquad (3)$$

This aggregated parameter is calculated from the local momentum fluxes themselves. Hence,

in the case of neutral thermal stratification, there is no difference between parameter aggregation and flux aggregation. When we consider stratified conditions, large differences between the two parameterizations occur, which cannot be neglected in numerical models.

We would like to illustrate the difference between parameter aggregation and flux aggregation by means of a simple example. Figure 1 shows the sensible heat flux at one single grid box of the ECHAM model in the inner Arctic ocean during winter time. The flux was calculated twice, once with parameter aggregation and once with flux aggregation, for varying fractional ice cover between open water and totally ice covered conditions. The atmospheric state was the same for all cases, i.e. no feedback between the heat flux and the atmospheric state was allowed. The temperature of the open water and sea ice were -1.9° C and -34° C, respectively. The temperature of the lowest level of the atmosphere model at approximately 30 m was -25° C and the windspeed 2 m/s. On the left and the right-hand side the values for open water and a total ice covered ocean appear. The heat flux over compact sea ice where the atmosphere is stable stratified almost vanishes (2 W/m^2), while over open water the flux becomes intense (-180 W/m^2). When a fractional sea-ice cover is considered, the resulting sensible heat flux simply is the linear interpolation between these two extreme cases when we apply flux aggregation. For the case of parameter aggregation the behaviour is quite different. For a sea-ice cover of more than 65 % the heat flux becomes almost zero. Below that ice concentration, the horizontal averaged stratification becomes unstable and the heat transfer is more intense. The kink in the respective curve is caused by a transition from the unstable to the stable regime.

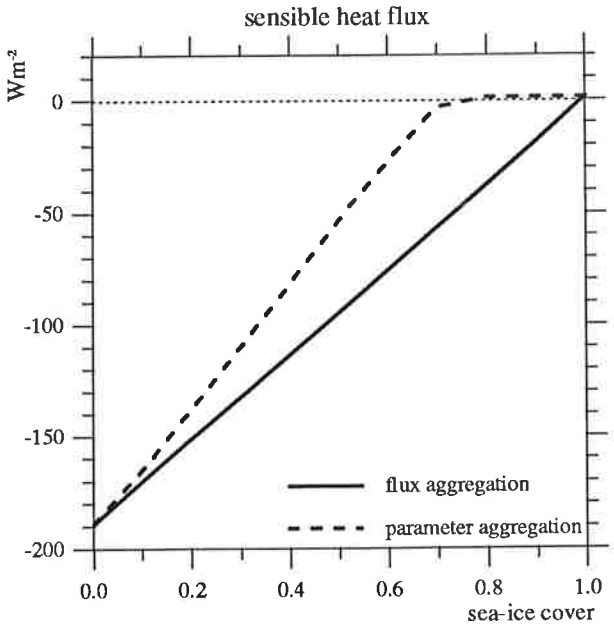

Figure 1: The turbulent sensible heat flux at the surface [W/m^2] as function of the fractional sea-ice cover for parameter aggregation and flux aggregation.

The sensible heat flux in the case of parameter aggregation is always smaller than with flux aggregation. Thus, the effect of the leads is underestimated when the surface temperature is lineary averaged. Especially for rather dense sea-ice cover the relative errors are remarkable. Nevertheless, the difference between the two parameterization techniques depends on the meteorological conditions. When the wind is more intense, turbulence is determined more by windshear and not by thermal stratification. Then, the differences will be smaller.

The difference between flux aggregation and parameter aggregation is mainly caused by the nonlinear dependency of the heat flux on the stratification, which has a strong impact when the stratification changes from a stable to an unstable regime. Within each regime the nonlinearities are not that important. An extreme case is when the temperature of the lower atmosphere is near ice temperature. If the parameter aggregation is applied the change of the large scale averaged stratification from unstable to stable conditions would happen at quite high fractional ice cover, i.e. the kink in the parameter aggregation curve in Figure 1 would be rather close to the right edge of the plot. The sensible heat flux then is almost everywhere in the unstable regime and the differences between the two parameterizations are quite small. An analogous result is achieved for the opposite extrem case where the lower air temperature is close to the temperature of the open water or higher.

We have introduced the technique of flux aggregation into the atmospheric general circulation model ECHAM3. The turbulent surface fluxes of momentum and heat are estimated for each surface category separately. The computation of these local fluxes should be done at the blending height. This height has been suggested to be dependent on the height of the planetary boundary layer, on patch dimensions, on the height of respective obstacles, or on the diffusion height scale. Typical values range from a few metres up to a hundred metres for the planetary boundary layer. Since there are a lot of uncertainties in the determination of this height, we calculate the turbulent fluxes at the lowest level of the atmospheric model, which, in the case of ECHAM3, has an altitude of approximately 30 m. Since the roughness lengths of sea ice and open water do not differ strongly, computation of turbulent fluxes at any level within the surface layer seems to be a fair approximation, provided the height of this level and the blending height are of the same order of magnitude (Claussen, 1991a). Grid averages of turbulent fluxes of momentum $[-\overline{(uw)}]$, sensible heat $[-\overline{(w\theta)}]$, and water vapour $[-\overline{(wq)}]$ are given by the average of local fluxes of each surface type weighted by its fractional area

$$
\begin{aligned}
[-\overline{(uw)}] &= f_{ice}\, C_m^{ice}(Ri_{ice}, z_{0_{ice}})\, U_{19}^2 + (1-f_{ice})\, C_m^{sea}(Ri_{sea}, z_{0_{sea}})\, U_{19}^2 \\
[-\overline{(w\theta)}] &= f_{ice}\, C_h^{ice}(Ri_{ice}, z_{0_{ice}})\, U_{19}\, (\Theta_{19}-\Theta_{ice}) + (1-f_{ice})\, C_h^{sea}(Ri_{sea}, z_{0_{sea}})\, U_{19}\, (\Theta_{19}-\Theta_{sea}) \qquad (7) \\
[-\overline{(wq)}] &= f_{ice}\, C_h^{ice}(Ri_{ice}, z_{0_{ice}})\, U_{19}\, (Q_{19}-Q_{ice}) + (1-f_{ice})\, C_h^{sea}(Ri_{sea}, z_{0_{sea}})\, U_{19}\, (Q_{19}-Q_{sea})
\end{aligned}
$$

where "***ice***" denotes the ice-covered part of a grid cell and "***sea***" stands for the open water.

C_m and C_h are the stability dependent bulk transfer coefficients for momentum and heat, respectively. The subscript ***19*** denotes the lowest level of the model.

The blending-height concept originally has been designed for turbulent fluxes. In extension we also calculate the solar radiation F_s and the thermal radiation F_T absorbed by the surface separately for each surface type.

$$\begin{aligned} [F_S] &= f_{ice}\,(1-\alpha_{ice})\,S \quad + (1-f_{ice})\,(1-\alpha_{sea})\,S \\ [F_T] &= f_{ice}\,(\varepsilon\,\sigma\,T_{ice}^4 - F_{\downarrow}) \quad + (1-f_{ice})\,(\varepsilon\,\sigma\,T_{sea}^4 - F_{\downarrow}) \end{aligned} \tag{8}$$

But we assume that the overlying atmosphere is in horizontal equilibrium. This implies that the incoming short wave radiation S and the downward long wave radiative flux $F_{\downarrow}$ are the same over sea-ice and open water. This might be correct as long as leads and ice floes are small and randomly distributed. At larger scales, for example at the ice margin or over large polynyas, these assumptions might no longer be correct.

An additional complication arises, if one takes into account that an ocean covered with sea ice is never a plain surface. Sea ice exhibits a certain freeboard depending on the thickness and history of ice. The sea-ice surface is deformed by pressure ridges caused by the movement of ice. These obstacles exert an additional form drag to the flow, resulting in a much stronger momentum flux than it would be expected from the individual surface roughness of sea ice and water alone. Thus, the effective roughness of such an area depends on the freeboard, size, and frequency of the ice floes, the silhouette area and the frequency of the pressure ridges, and the local skin frictions. The total momentum transport over such an area cannot be determined from local fluxes as described before.

The total wind stress over a heterogeneous area of sea ice can be obtained by applying the drag partition theory (Arya 1975). The turbulent heat fluxes on the other hand are not directly affected by the form drag of such elements. Therefore, Claussen (1994a) suggests evaluating only large-scale momentum fluxes from the large-scale roughness including the sea-ice freeboard, whereas the turbulent heat fluxes should still be estimated from local surface properties. A complete description of this procedure including the ice freeboard and stability effects is given in Stössel and Claussen (1993).

We performed sensitivity experiments with the atmospheric general circulation model ECHAM3 in order to study the influence of sea-ice freeboard on the momentum transfer and the atmospheric circulation. The results showed no significant impact on the climate of the atmospheric model. It seems, that the atmospheric circulation is not very sensitive to the surface- roughness parameterization in high latitudes. Therefore, we decided to neglect the effect of freeboard in the parameterization of sub-grid scale sea ice. The consideration of the

influence of ice freeboard on the momentum transport is much more important for dynamical sea-ice modelling (Stössel and Claussen, 1993), because the windstress is a very important component of the momentum budget of the sea ice.

As mentioned before, the blending-height concept is a result of investigations in the micro-scale. It is valid as long as the length scales of the surface heterogeneties are quite small, say in the order of hundreds of meters, and only the lower boundary layer of the atmosphere is directly involved. When the heterogeneities get larger, they are felt at larger heights and the concept is not applicable any more. Phenomenona like meso-scale circulations, convection, or different clouds for different surface types have to be considered. Nevertheless the exact limitations of the concept are not well known (Claussen, 1994b). But since a large amount of the sea-ice distribution is contained in the smaller scales the blending-height concept is an acceptable approach for our application.

4. Experimental design

In this paper we investigate the impact of sub-grid scale sea-ice inhomogeneities on the ECHAM3 model results. Especially, we would like to answer three questions:

1. How do the sea-ice surface temperature, and the surface fluxes of momentum, heat, and water vapour over areas covered with sea ice change when leads are allowed compared to a situation with a total dense ice cover? This question addresses the problem of correctly coupling an atmosphere model to an ocean model.

2. Has the inclusion of leads into the sea ice any impact on the local and remote structure of the atmospheric circulation? The introduction of the leads into the sea-ice results in an increase of the "effective" sea-surface temperature and thus provides an additional heat source for the atmosphere.

3. Can there be a difference detected in the response of ECHAM3 to different parameterizations of sea-ice inhomogeneities, i.e. have the simple averaging of surface parameters and the more sophisticated flux aggregation concept a different impact upon the model climate?

In order to answer these questions a series of numerical experiments was carried out. In each experiment identical fractional sea-ice distributions were prescribed (Figure 2). As observational data of this variable were not available with desired detail, we used model output from a coupled atmosphere-ocean model (Lunkeit et al., 1994). The margin of this simulated sea-ice cover is more northward than in observations. However, as we are only

interested in the sensitivity of the model climate to various parameterizations and not in simulating the real atmosphere, the exact choice of the sea-ice data is not important in our case. The sea-ice thickness in the Northern and Southern Hemispheres were fixed to 2 m and 1 m, respectively.

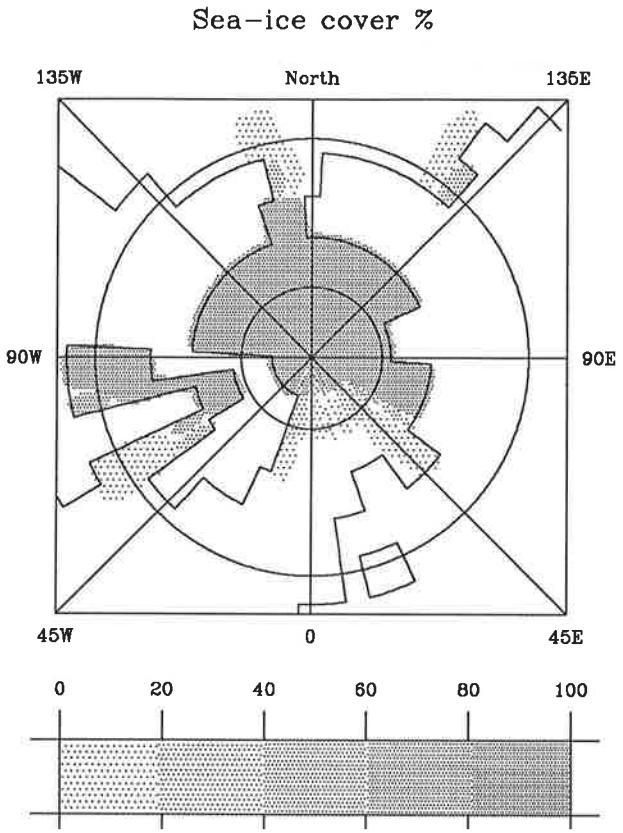

Figure 2: The fractional sea-ice cover of January as used in the sensitivity experiments. The two circles indicate 60° N and 80° N.

Using always the same sea-ice distribution we have performed four numerical experiments with different parameterizations of the air-sea fluxes in the sea-ice covered areas:

CONTROL A sea-ice parameterization analogous to the operational version of ECHAM3 was chosen, i.e. any ocean grid box is either totally ice-covered or free of ice. A grid box is regarded as ice-covered if the fractional sea-ice cover is larger than 10 %.

PARAM An averaging of surface parameters, logarithmic for the roughness lengths and linear for all other parameters, was applied to get representative grid averages ("parameter aggregation").

FLUX An averaging of the surface fluxes according to equation (4) was applied ("flux aggregation").

NOICE Every grid-box was free of sea ice. Several experiments in literature (i.e. Newson, 1973; Royer et al., 1990) adressed the problem of possible impacts of an ice-free Arctic on the atmospheric circulation. We included such an experiment, which represents the opposite extreme of the control experiment with totally ice-covered grid-boxes for the purpose of comparison.

The sea-surface temperature was set to -1.7 °C at those points, where the fractional sea-ice cover was lower than 100 %. All other conditions in the different experiments were the identical according to the AMIP dataset (Atmospheric Modelling Intercomparison Project; Gates, 1992). A T21 horizontal resolution was chosen. The experiments were performed in the perpetual January mode, i.e. the solar irradiance and the sea-surface temperature were fixed to January values, but the daily cycle remained included.

The model was integrated for 24 simulated months in each case. The first three months were discarded, as an initial spin-up occurs towards the individual quasi-equilibrium climate of each experiment. In the following we will present averages and differences between the experiments calculated on the bases of the last 21 months. Both, zonal means and horizontal distributions of relevant variables will be discussed.

The model climate exhibits a rather large internal (natural) variability. Thus the significance of differences between two simulations is checked by a local T-test on the 95 % and 99 % significance levels. Since the monthly means are not independent in a permanent January integration we also tested odd and even months separately. But this only had a slight influence on the results.

We will show only results from the winter hemisphere, which is the only region with a significant impact. In the Southern Hemisphere, the sea ice has approximately the same temperature as the water in the leads due to the rather high solar radiation in summer. Consequently, the turbulent fluxes are only slightly different between open water and sea ice. Therefore, the method of parameterization is not important. Only the surface albedo is increased significantly when leads are included in the sea ice. However, the higher absorption of solar energy is stored in the ocean, which has an unlimited heat capacity in a model with prescribed sea-surface temperature. Therefore, no relevant feedback to the atmosphere is expected. On the other hand considerable differences of the surface temperatures of sea ice and open water show up on the winter hemisphere, what makes us to concentrate on this hemisphere.

5. Results

5.1 Surface Temperature

During the Northern Hemispheric winter the leads directly cause an increase of the surface temperature. Figure 3 shows the horizontal distributions of the surface temperature for the control run and the sensitivity experiments. In the control run (Figure 3a) very cold temperatures are simulated over sea-ice covered areas with values below -30 °C, in some areas below -35 °C. In the sensitivity experiments (PARAM, FLUX) leads have been introduced according to the fractional sea-ice cover plotted in Figure 2. In the leads the sea-surface temperature was fixed 0.2 K above the freezing point of sea water. This temperature is quite high compared to the surface temperature of the surrounding sea ice. Figures 3b and 3c show the changes of the surface temperature relative to the CONTROL run as they were simulated in the sensitivity experiments PARAM and FLUX. For areas with fractional sea-ice cover, the grid mean of the surface temperature, i.e. the weighted average of the ice surface temperature and the lead surface temperature is displayed. In the case of flux aggregation (FLUX) the sea-ice surface temperature is significantly enhanced, in some areas up to 20 K. Even in the inner Arctic, where the leads cover only a small amount of the total surface, the temperature increase amounts to approx. 8 K. The increase of the surface-temperature cannot be explained by the high temperatures of the leads themselves, because they cover only a small fraction of the total area. The ice temperature is enhanced itself due to a modified energy balance of the ice, as we shall see later. In the case of parameter aggregation (PARAM) the temperature rise of the surface in sea-ice regions is much weaker. It reaches about 10-15 K near the sea-ice margin where the compactness is rather low. In the inner Arctic the temperature increase is almost neglectable. As expected, the changes of the surface temperature for the experiment with total removal of sea ice (NOICE) have the most intense impact on the model atmosphere. The very cold temperatures of the control run are replaced by temperatures at the freezing point of sea-water leading to temperature changes of more than 30 K in areas, which had been covered with sea-ice before.

The warming in the sensitivity experiments is not confined to the region were the forcing is imposed. The surface temperatures of the adjacent continents are also enhanced because the warming is spread out by advection and diffusion. The sea-surface temperatures are fixed according to the prescribed climatological distribution. In the NOICE experiment the warming reaches over Europe, Asia and Northern America down till 60° N, over the eastern part of America even till 50° N. Southwards slight coolings of about 1 K and 2 K in the maximum are simulated over Siberia and over America, respectively. The remote response of the surface temperature over Europe and Northern Asia is comparable to that in the experiment of Royer (1990), where the sea ice was totally removed. The cooling over

Northern America is not found in that experiment, they got a warming of the same amplitude. Considering, that they simulated only 90 days in their experiment and that the temperatures over the continents are highly variable, we think that the discrepancy is not significant. In the FLUX experiment the extension and amplitude of the warming over Asia are quite similar to that in the NOICE experiment. Over the western part of Northern America the warming is limited more northwards at 65° N. The significant fraction of cooling areas southwards over the continents are quite similar to those in the NOICE experiment. In the PARAM experiment only a slight warming over the continents is simulated and its statistical significance is rather low. The cooling over the southern part of Northern America is simulated quite similar to the other experiments.

Where the surface temperatures are increased in the sensitivity experiments PARAM , FLUX and NOICE, both over the leads and over the sea ice, the potential evaporation in the Artic is also increased. This leads to an enhanced input of water vapour into the polar atmosphere and an additional heating by the release of latent heat. The additional forcing due to higher surface temperatures and higher potential evaporation is restricted to areas originally covered with sea ice northwards of 60° N in all the sensitivity experiments.

5.2 Surface Fluxes

Due to the additional surface forcing in the sensitivity experiments, the surface heat fluxes are enhanced over sea-ice covered areas. Figure 4 shows the zonal means of the surface energy fluxes (sensible and latent turbulent heat flux, thermal radiation and net heat flux; the solar radiation is neglectable in a January experiment) as simulated in the CONTROL run and the three sensitivity experiments PARAM, FLUX and NOICE. Since pressure coordinates are applied in the model, negative values denote fluxes directed upwards. At high latitudes the turbulent heat fluxes are enhanced in all the sensitivity experiments. The zonal mean of the sensible heat flux at the ice edge, where the compactness is quite low, is increased by about 10 W/m^2 in the case of parameter aggregation (PARAM) while no change is simulated in the inner Arctic (Figure 4a). In the case of averaging the fluxes (FLUX) a larger increase of about 17 W/m^2 is visible at the sea-ice margin. Compared to the CONTROL run, the sign of the flux changed and is now directed upward. A pronounced difference between the sensitivity experiments is found in the inner Arctic where the compactness of the sea ice is typically around 95 %. In the case of FLUX the zonal mean of the sensible heat flux increased by about 10 W/m^2 and is now directed upwards. This clearly demonstrates the importance of even small leads in the sea ice for the overall stability and for the energy exchange. This non-linear behaviour cannot be represented by simply averaging the surface parameters.

As expected the response of the sensible heat flux in the NOICE experiment is much

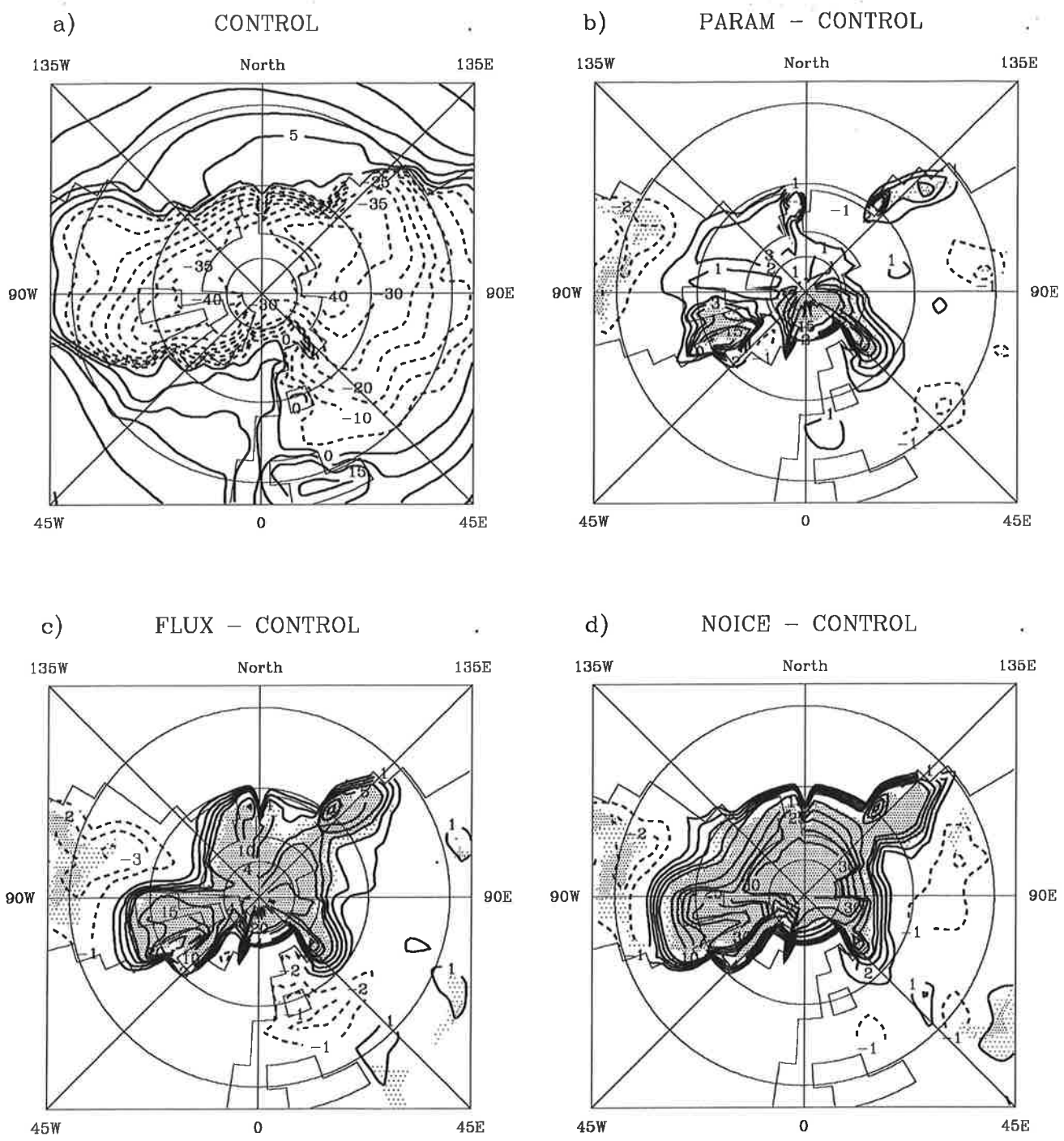

Figure 3: Horizontal distributions of the surface temperature [°C] for the control experiment (CONTROL) and their changes in the experiments with parameter aggregation (PARAM minus CONTROL), flux aggregation (FLUX minus CONTROL) and the total removal of the sea ice (NOICE minus CONTROL). The contour interval in Fig. a is 5 °C. In the difference plots contours are shown for ±1, ±2, ±3, ±4, ±5, ±10, ±15, ±20, ±25, ±30 °C. The light and dark shadings show those areas, where the changes are significant at a 95 % and 99 % level, respectively, according to a local t-test.

stronger. Changes of 40 W/m^2 occur relative to the CONTROL experiment. The response in the FLUX experiment is three times smaller, but compared to that in the PARAM experiment still remarkable, having in mind the rather compact sea-ice cover in the inner Arctic. The NOICE experiment also shows at 75° N a strong enhancement of the sensible heat flux, while in the experiments with sub-grid scale sea-ice distribution no change is observed. As we shall see later when we discuss horizontal distributions of the sensible heat flux, the flux over areas with sea-ice cover at 75° N like the Hudson Bay and Labrador Sea is also enhanced in those experiments. But in the zonal mean this is compensated by a reduction of the sensible heatflux southwards of the ice edge, especially in the Norwegian Sea. This is consequence of the reduced horizontal temperature gradient at the sea-ice margin. The enormous heat fluxes southwabds of the sea-ice margin are caused by cold air coming from the Arctic sea ice blowing over the relatively warm open water of the northern oceans. The great temperature difference between water and the air leads to strong upwards directed fluxes in those regions. Therefore, a weakening of the horizontal temperature gradient in those areas results in a reduction of turbulent heat transfer, compensating the enhancement over different areas at the same latitude.

The reduced advection of cold air is the cause for the simulated slight reduction of heat transfer from the ocean to the atmosphere in the mid latitudes in all the sensitivity experiments. Moreover, the surface windspeed in mid-latitudes is also reduced in the FLUX and NOICE experiments, as we shall see later. This also results in a reduction of turbulent heat transfer.

The latent heat fluxes (Figure 4b) show a similar sensitivity, the increase in high latitudes and mid latitudes is comparable to that of the sensible heat flux. Both, the meridional structure and the amplitudes, look quite similar for all the sensitivity experiments. This is not surprising since the exchange of water vapour is mainly determined by the surface temperature.

As a consequence of the enhanced surface temperature the emitted longwave radiation (Figure 4c) is increased substantially about 5 W/m^2 in the case of parameter aggregation and by 10 W/m^2 in the case of flux aggregation. The difference between the two sensitivity experiments is not a result of the non-linear dependency of the longwave radiation on the surface temperature. In the temperature range considered here the impact of the non-linearity according to the Stephan-Boltzmann-law is almost negligible. The stronger longwave radiation in the case of flux aggregation is caused by a higher surface temperature of the sea ice itself (see Figure 3). The much higher forcing of the surface temperature in the NOICE experiment causes an increase of the longwave emission of about 50 W/m^2.

In our experiments the sensitivity of the surface fluxes to a total removal of the sea ice is

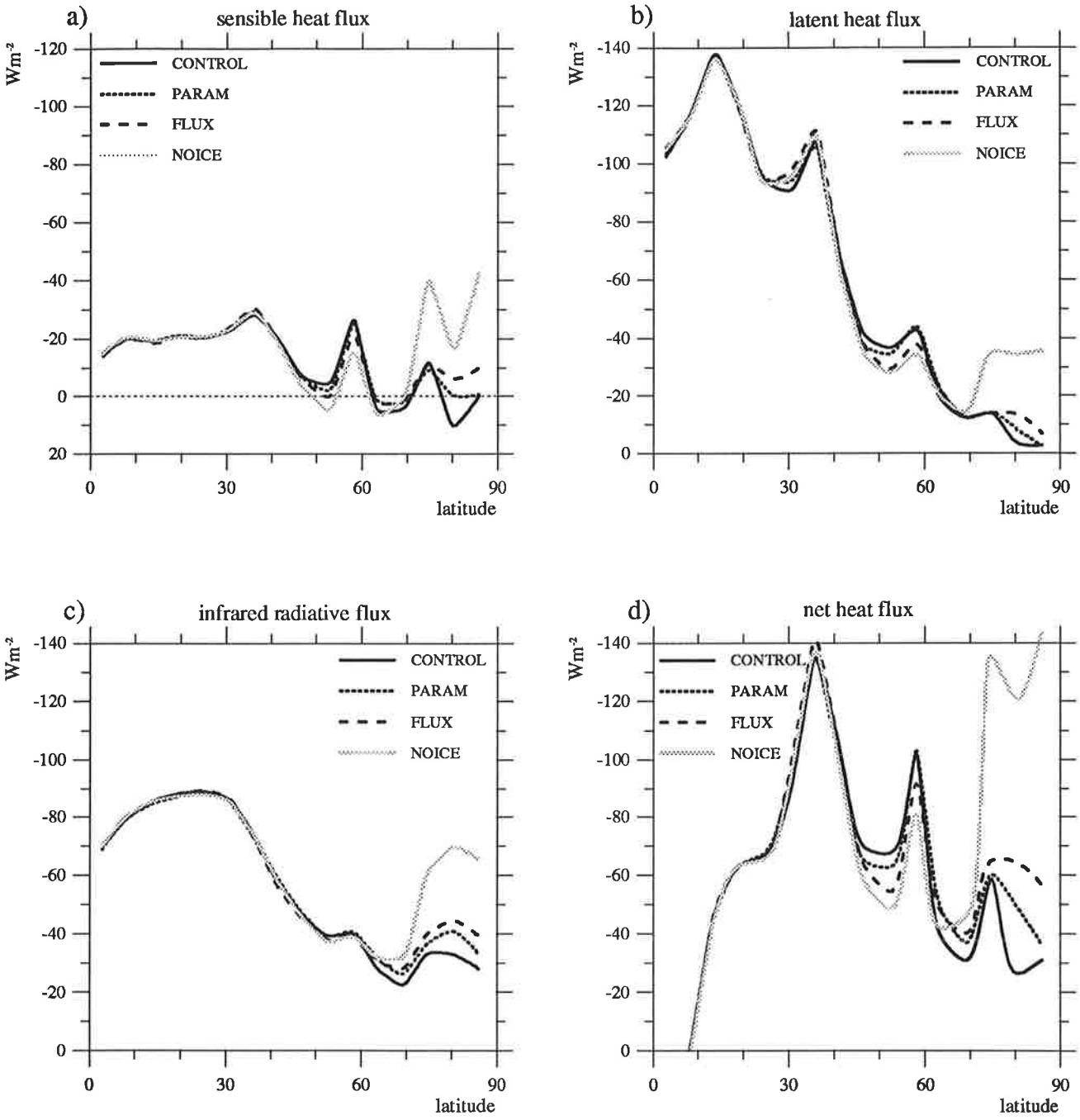

Figure 4: Zonal mean distributions of the surface fluxes of sensible and latent heat, the infrared radiative flux and the net heat flux [W/m^2] for the different experiments. Negative values denote fluxes that are directed upward.

much stronger than in that of Royer et al. (1990). This is not surprising since the temperatures of our control case are considerably lower resulting in a more intense forcing in the sensitivity experiment.

The sum of the fluxes of sensible, latent heat and radiation (now including the solar radiation) gives the total energy flux from the atmosphere to the ocean (Figure 4d). In the case of parameter aggregation (PARAM) the net heat flux increased about 23 W/m^2 at the ice edge and about 5 W/m^2 in the inner Arctic. For the FLUX experiment the numbers are 40 W/m^2 and 25 W/m^2 respectively, resulting in a net heat input into the atmosphere of more than 50 W/m^2 for high latitudes. This number is similar to results obtained by Nakamura and Oort (1988) from observations by studying the energy budget of the polar regions. The corresponding number for the NOICE experiment is a heat loss of the polar ocean in the order of 130 W/m^2. This enormous heat flux seems to be quite unrealistic. This clearly shows that it is not reasonable to study the problem of an ice-free Arctic ocean in a pure atmosphere model. The polar ocean would react to such a strong forcing with formation of sea ice and realistic results can only be obtained in a coupled ocean-atmosphere model.

The dynamic response of the ECHAM atmosphere has a distinct non-zonal structure. Thus we discuss the horizontal distribution of the model reponse and show maps in stereographic projection of the main interesting atmospheric variables. Sections reaching from the pole down to 35° N will be shown. The tropics are not included because in that region no impact is caused by the forcing in the Arctic.

The Figure 5 illustrates the sensitivity of the sensible heat flux in more detail. Figure 5a shows the spatial pattern of the flux of sensible heat for the CONTROL experiment. The changes in the sensitivity experiments PARAM, FLUX and NOICE are plotted in the Figures 5b-d. The most dramatic changes happen in the Norwegian Sea, in the Hudson Bay, and Labrador Sea. The changes are similar for the three sensitivity experiments and reach values up to 100 W/m^2. In those regions, the compactness of the sea-ice is quite low and therefore, the sensitivity in all experiments is almost the same. In the inner Arctic, the change of the sensible heat flux almost vanishes in the case of parameter aggregation (PARAM), while differences up to 20 $W/m^2$are simulated for the case of flux aggregation (FLUX). The latter alters the direction of the flux, which is in some places it is now directed upwards indicating the dominance of the unstable stratification above the leads over the stable stratification above the sea ice. In the NOICE experiment the flux in the regions which had been covered with ice is now generally directed upwards. The changes generally exceed 20 W/m^2.

The regions southward of the sea-ice margin, where the sensible heat flux is reduced by a remarkable amount, are clearly identified. Typical values for flux aggregation (FLUX) are

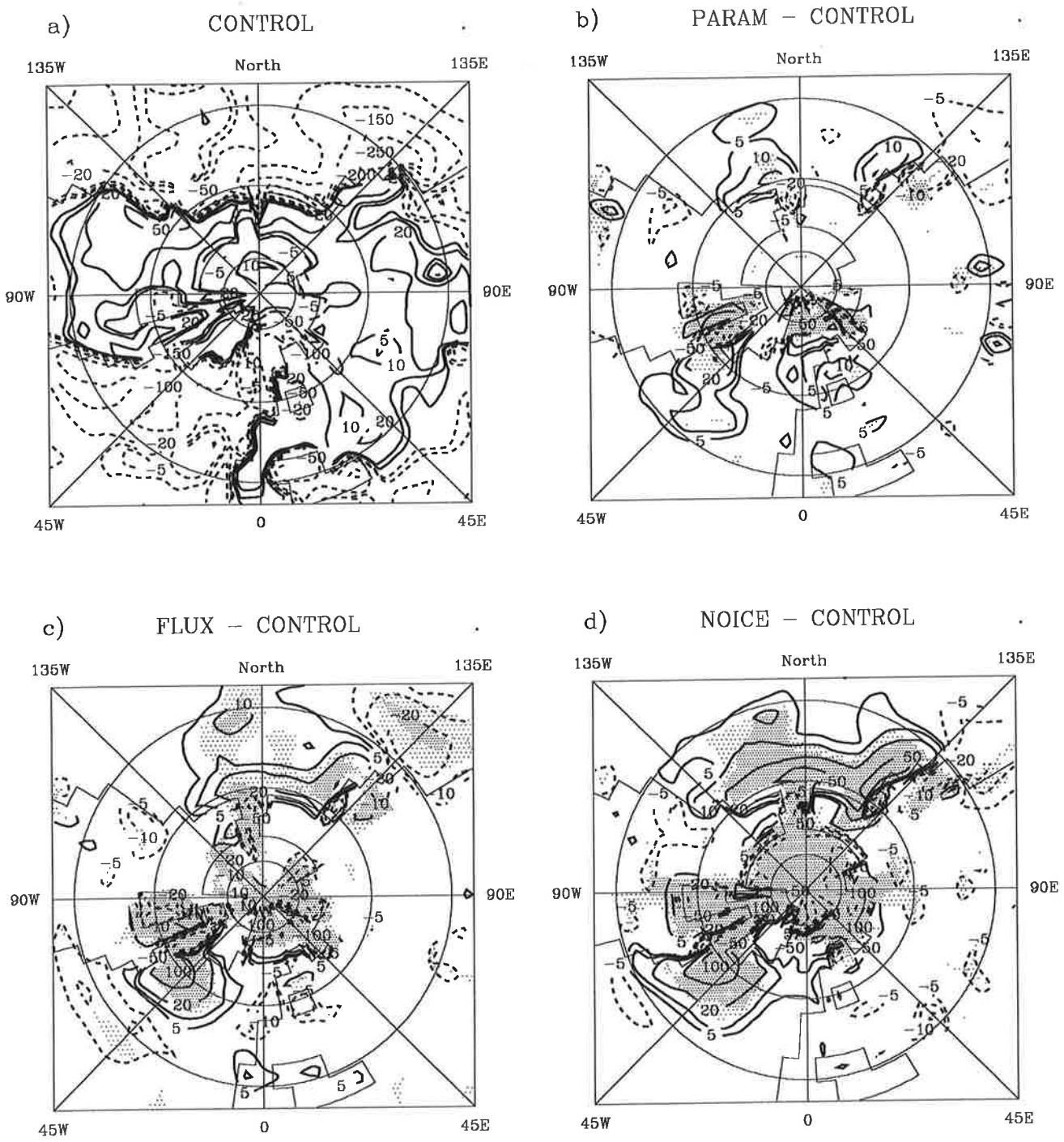

Figure 5: Horizontal distributions of the surface sensible heat flux [W/m^2] for the control experiment (CONTROL) and their changes in the experiments with parameter aggregation (PARAM minus CONTROL), flux aggregation (FLUX minus CONTROL) and the total removal of the sea ice (NOICE minus CONTROL). The contour intervals are ±5, ±10, ±20, ±50, ±150, ±200, ±250 W/m^2. The light and dark shadings show those areas, where the changes are significant at a 95 % and 99 % level, respectively, according to a local t-test.

20 W/m^2 but extreme reductions of 100 W/m^2 can be achieved like at the east coast of Northern America. The reductions southwards of the ice edge in the Western hemisphere are quite similar in the NOICE experiment. In the Pacific region the spatial extent of the reduction is much larger and extreme reductions of 50 W/m^2 are simulated. In the case of parameter aggregation the weakening of the heat transfer can also be identified. Nevertheless, it is much less pronounced as the horizontal temperature differences at the sea-ice margin are much smaller. Both in the FLUX and in the NOICE experiment, an intensification of about 20 W/m^2 is simulated in the Japanese Sea. This is a result of higher windspeeds and a stronger advection of cold air from the Asian continent due to an intensification of the Aleutian low as we shall see in the discussion of the pressure fields. Over land the changes in the sensible heat flux are almost negligible for all the sensitivity experiments. Thus, the change will mainly affect the energetics of the underlying oceans. The heat transfer from the ocean is reduced southwards of the ice margin and enhanced in the sea-ice regions. The result is a northwards shift of the zeroline in the energy exchange. In a coupled ocean-atmosphere model this effect would have strong consequences for the development of the ice cover. It could be expected that the ice cover should be restricted to a more limited area than without consideration of sub-grid scale sea-ice inhomogeneities, if tuning parameters remain unchanged. But this questions can only be adressed in experiments using coupled models .

In the sensitivity experiments presented here no significant modifications of the momentum transfer were simulated. The surface roughness over fractional sea ice was rather crudely parameterized by just aggregating the local roughness lenghts of sea ice and open water. The roughness of the ice was fixed at 10^{-3} m, the roughness of the water was parametrized depending on the low level wind according to the Charnock-formula (Charnock, 1955). Since these local roughness lengths did not differ that much, it is not surprising, that no impact on the momentum transfer by the aggregated surface rougness could be obtained. When the additional surface drag imposed by the ice freeboard is taken into account, the effective roughness over sea ice is effectively enhanced. Additional sensitivity experiments showed an increase of the effective surface roughness by more than 50 % due to the ice ridges depending on the compactness of the ice. Nevertheless, the impact on the surface momentum budget was quite small. Only minor changes with little statistical significance were simulated. It appears to us, that the low level winds partly adjust resulting in an almost unmodified surface stress. The conclusion that the sensitivity of the atmospheric circulation related to the surface roughness in high latitudes is quite small and its parameterization is not that important for realistic simulation results. The parameterization of the surface roughness in sea-ice covered regions is much more important for the forcing of an underlying ocean and the sea ice itself. This has been clearly been demonstrated by Stössel and Claussen (1993), who simulated the Antartic sea-ice cover with an interactively coupled dynamical sea-ice model.

5.3 Zonal Mean Temperature

Figure 6 shows latitude-height cross-sections of the zonal mean temperature. The enhanced heat input at the lower boundary at high latitudes warms the atmosphere significantly in the case of flux aggregation (FLUX), with a maximum of 7 K near the surface at the pole. The warming extends up to the tropopause. In the stratosphere, a cooling of about 2 K is simulated. Nevertheless, due to the internal variability of the data the warming is statistical significant only up to 700 hPa, where a temperature difference of 1 K is found. The warming extends southward to 50° N. In the case of parameter aggregation, the warming is restricted to the lowest part of the atmosphere with a maximum of only 3 K. The warming is significant up to 900 hPa. In the experiment without sea-ice (NOICE) the warming of the boundary layer is very strong with extreme values of 30 K at the surface. As in the FLUX experiment the warming is essentially confined to the boundary layer. The extent is slightly larger reaching up to 600 hpa in the vertical and till 45° N. The similarity in the spatial extension of the temperature response between the NOICE and the FLUX experiment is quite surprising and clearly demonstrates the importance of leads in the sea ice in an atmospheric climate model.

It should be pointed out that in the case of flux aggregation the stronger warming of the atmosphere should increase the large scale stability of the boundary layer and therefore reduce the turbulent heat exchange. Despite of this large scale stability increase the turbulent fluxes are still much higher than with parameter aggregation. This shows again the effectivity of even small leads for the transport of heat and water vapour from the ocean to the atmosphere.

The slight cooling above and southwards of the warming region due to adiabatic processes, which has been reported by Royer et al. (1990) is not confirmed by our experiments. Our experiments show only small modifications in those regions with different sign. The variability of the data is quite high in that areas. Therefore clear conclusions cannot be drawn.

5.4 Energy Budget

If leads are included in the sea-ice parameterization, the energy input from the surface into the atmosphere is enhanced and the atmospheric temperature is higher. This modifies the energy budget of the Arctic region. At the top of the atmosphere, only the long wave radiative flux contributes to the energy budget under January conditions. As the surface temperature is increased, we should expect an enhanced long wave radiative loss of the polar atmosphere. Indeed, for the case of flux aggregation (FLUX) the longwave radiation at the top of the atmopsphere is 9 Wm^{-2} higher than in the CONTROL run (see Figure 7). This

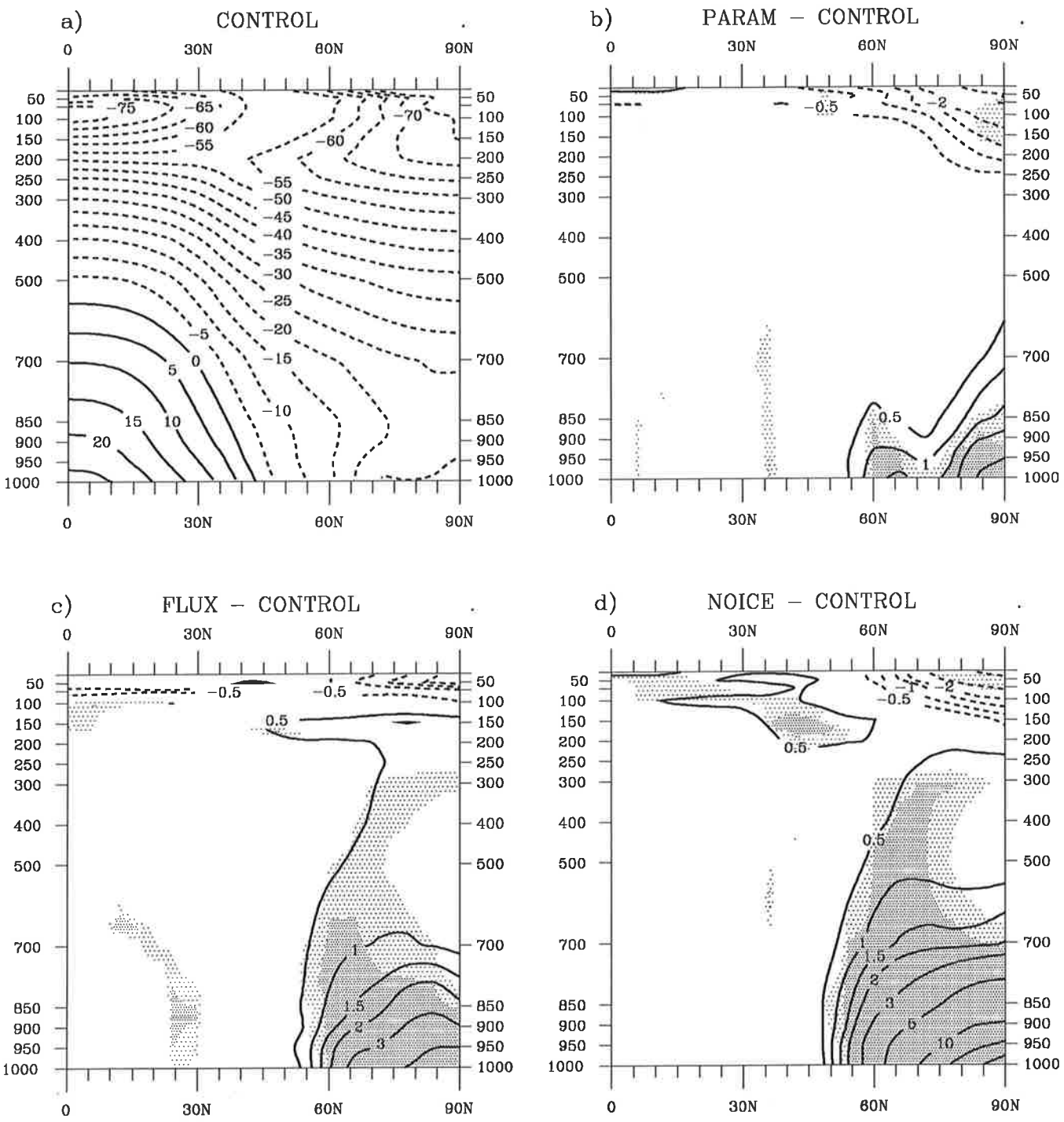

Figure 6: Latitude-height distributions of the zonally averaged January temperature [°C] for the control experiment (CONTROL) and their changes in the experiments with parameter aggregation (PARAM minus CONTROL), flux aggregation (FLUX minus CONTROL) and the total removal of the sea ice (NOICE minus CONTROL). The contour interval in Fig. a is 5 °C. In the difference plots contours are shown for ±0.5, ±1, ±1.5, ±2, ±3 ±5, ±10, ±15, ±20 °C. The light and dark shadings show those areas, where the changes are significant at a 95 % and 99 % level, respectively, according to a local t-test.

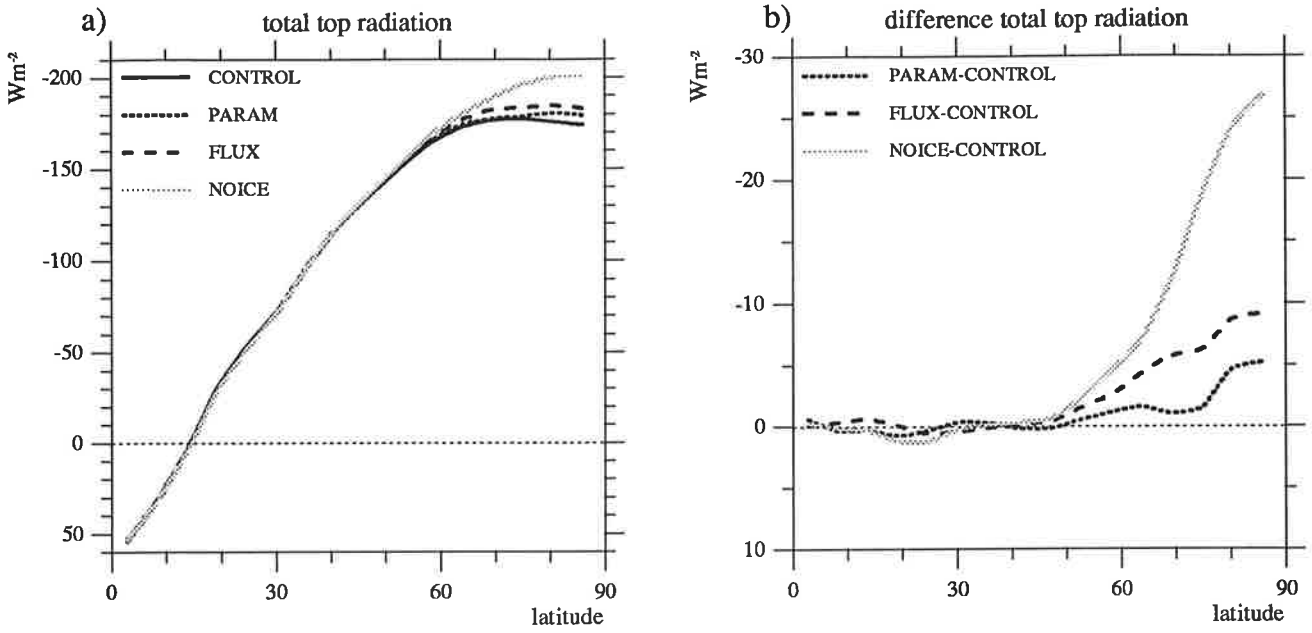

Figure 7: a.) Zonal mean distributions of the radiation at the top of the atmosphere [W/m^2] for the different experiments; b.) changes of the radiation relative to the control experiment.

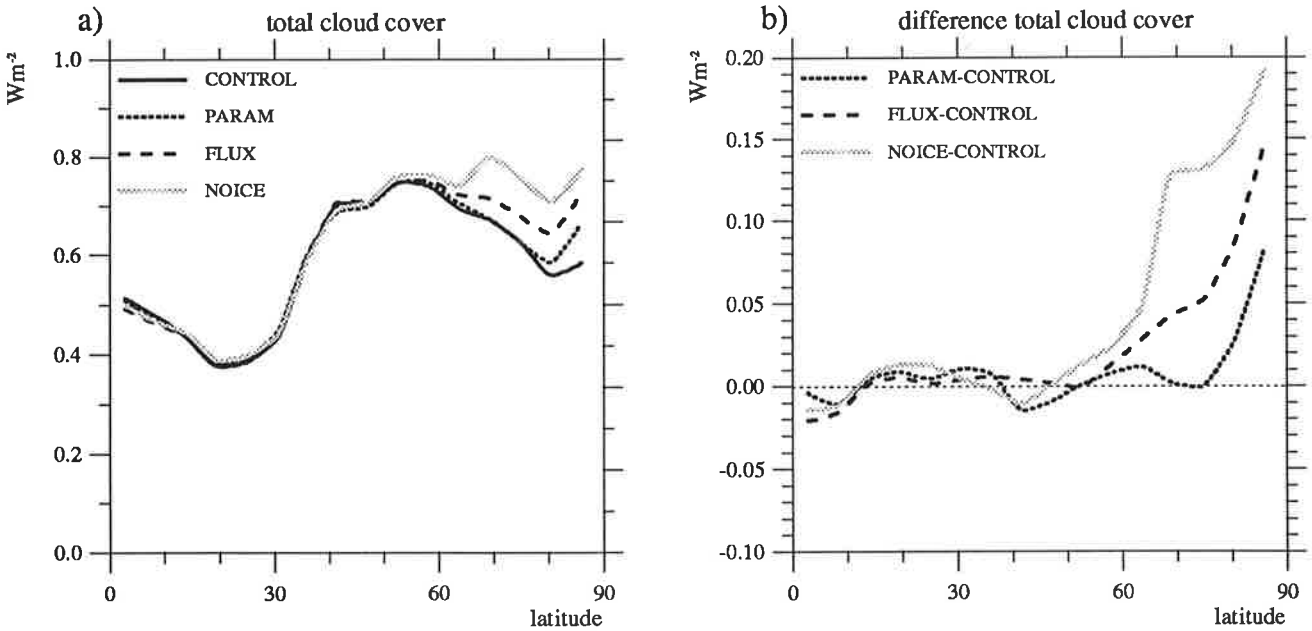

Figure 8: a.) Zonal mean distributions of the total cloud cover [%] for the different experiments; b.) changes of the cloud cover relative to the control experiment.

increase amounts to 6 % of the total flux. In the case of parameter aggregation the difference is only 5 W/m^2. In both cases the increase at the top of the atmosphere is smaller than the rise of the corresponding surface flux. This difference can be explained by an increase in the total cloud cover over the arctic region (Figure 8). The cloud cover is enhanced by 0.1-0.15 and 0.05 in the case of flux aggregation and parameter aggregation, respectively. The additional clouds are caused by the higher input of water vapour through the leads. The higher cloudiness weakens the increase of thermal radiative loss by additional absorption in the atmosphere. When the sea ice is totally removed (NOICE), the total radiative loss is much stronger. Due to the high surface temperatures the thermal radiation emitted to space is enhanced by approximately 30 W/m^2. This is smaller than the changes at the surface, where the numbers are always higher than 40 W/m^2. Again the cause is an increase in the total cloud cover. The cloudiness changed from 0.6 in the CONTROL case to almost 0.8 in the NOICE experiment. This greenhouse effect caused by additional cloudiness and water vapour also explains the cooling of the polar stratosphere mentioned before.

As we saw above (Figure 3), the sea-ice surface temperature rises in the experiments with fractional sea-ice cover. The atmosphere above the sea-ice warms due to the rather effective additional heat input through the leads. This enhances the sensible heat flux from the atmosphere to the sea-ice. Moreover, the atmospheric radiation is enhanced by higher atmospheric temperatures and the increased cloudiness. These effects are much stronger in the case of flux aggregation than in the case of parameter aggregation, which results in considerable higher sea-ice surface temperatures in the first case.

5.5 Zonal wind

The higher temperature over the Arctic weakens the meridional temperature gradient and consequently also the meridional pressure gradient. This influences the dynamics of the circulation in polar latitudes. However, in the case of parameter aggregation (PARAM) the weakening of the meridional gradients is not pronounced enough to have a significant impact on the zonal wind (Figure 9b). When we apply flux aggregation (FLUX), the warming covers the whole polar troposphere and reduces the meridional gradient of the geopotential height. The result is a weakening of the westerly flow in the midlatitudes (Figure 9c). The position and strength of the sub-tropical jet is not affected but between 50° N and 70° N the zonal wind is significantly reduced throughout the whole troposphere. The maximum reduction of 2.5 m/s is found between 100 hPa and 300 hPa. In the lower troposphere, the reduction exceeds 20 % of the absolute windspeed in the CONTROL run. The slight increase of the wind in the sub-tropical region seems to be connected with a slight southwards shift of the sub-tropical jet. But this feature is not statistically significant. It is very interesting, that the response of the zonal wind in the NOICE experiment (Figure 9d) is quite similar to that in the FLUX experiment. As shown before, the structure of the warming looks quite similar in

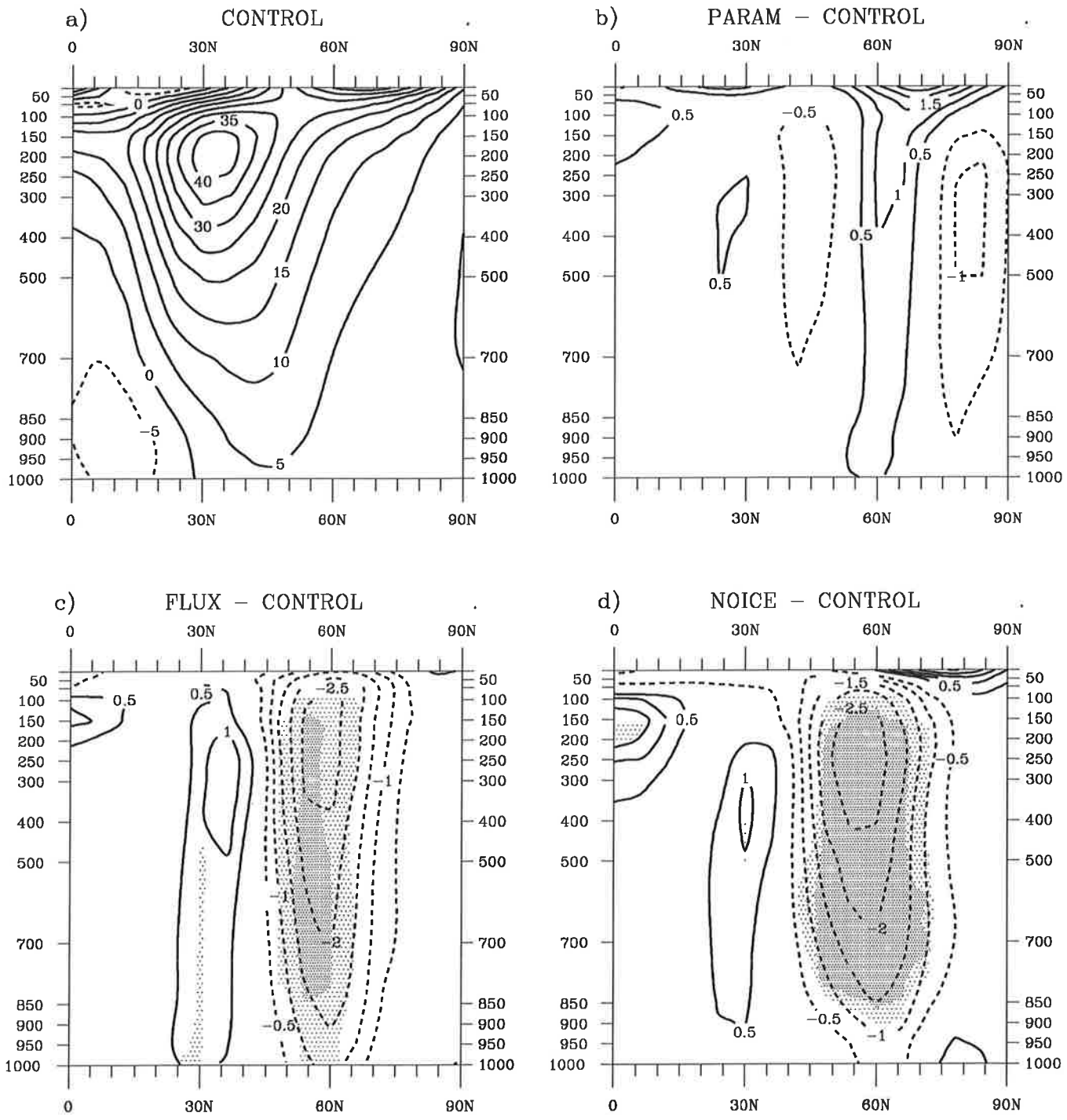

Figure 9: Vertical distributions of the zonally averaged zonal wind [m/s] for the control experiment (CONTROL) and their changes in the experiments with parameter aggregation (PARAM minus CONTROL), flux aggregation (FLUX minus CONTROL) and the total removal of the sea ice (NOICE minus CONTROL). The contour interval in Fig. a is 5 m/s. In the difference plots contours are shown for ±1, ±1.5, ±2, ±2.5 m/s. The light and dark shadings show those areas, where the changes are significant at a 95 % and 99 % level, respectively, according to a local t-test.

both experiments. The main differences are confined to the near surface layer. Further above, the warming is quite similar and thus the responses of the geopotential height field and the zonal wind are almost the same.

5.6 Temperature at 850 hPa

The horizontal structure of the tropospheric warming for the different sensitivity experiments is illustrated by the 850 hPa temperature response (Figure 10). The deviations from the zonal mean are apparent. The maxima of the temperature response resemble the distribution of the surface forcing. In the experiment with parameter aggregation (PARAM) the impact is only very weak and always below the internal variability of the model. Nevertheless, the two maxima of warming with 1 K over the Labrador Sea and with 2 K at the ice edge east of Greenland can directly be related to the enhanced heat input from the surface below. Over Alaska, the temperatures are also slightly increased which might be related to the ice reduction in the Bering Sea. Over the rest of the Arctic, the changes are only very small.

The other two experiments (FLUX, NOICE) exhibit a much stronger response. Their temperature change looks quite similar with three maxima. The most dramatic changes happen over the Labrador Sea with warmings of 6 K for flux aggregation and 10 K for the ice free experiment. Two smaller maxima appear over the central Arctic and the Sea of Ochotosk with amplitudes of approximately 2 K for the FLUX experiment, and 8 K and 4 K for the NOICE experiment. These local warmings, which are directly caused by the additional surface heat input are transported to the adjacent areas by diffusion and advection. At the western slopes of the Northern American and the Northern Pacific troughs the warming is transported to the south while on the eastern side of the Northern American trough the warming is restricted to the high latitudes. In both experiments a small warming of more than 1 K appears at the eastern side of the Pacific trough which cannot directly be attributed to the changes in the Artic, because the flow in that area is northerly directed. As we shall see later, the Northern Pacific trough is intensified in both experiments. Therefore, more warm air is advected from lower latitudes into the area south of Alaska and contributes to the tropospheric warming. Also the minor cooling over the Japanese Sea in both experiments can be explained by an enhanced advection from the cold Asian continent due to the intensified trough. This feature is also confirmed by the strong increase of the turbulent heat loss of the ocean at the coast in the Japanese Sea.

In the experiment with parameter aggregation no clear changes in the 850 hPa temperature can be detected outside the Artic. This is not surprising in view of the weak signal in the Artic itself. A significant cooling of more than 1 K is only simulated in the southern part of Northern America. This cooling also appears in the two other experiments. The cause is not clear. It might be advective, as the wind over the American continent becomes slightly more

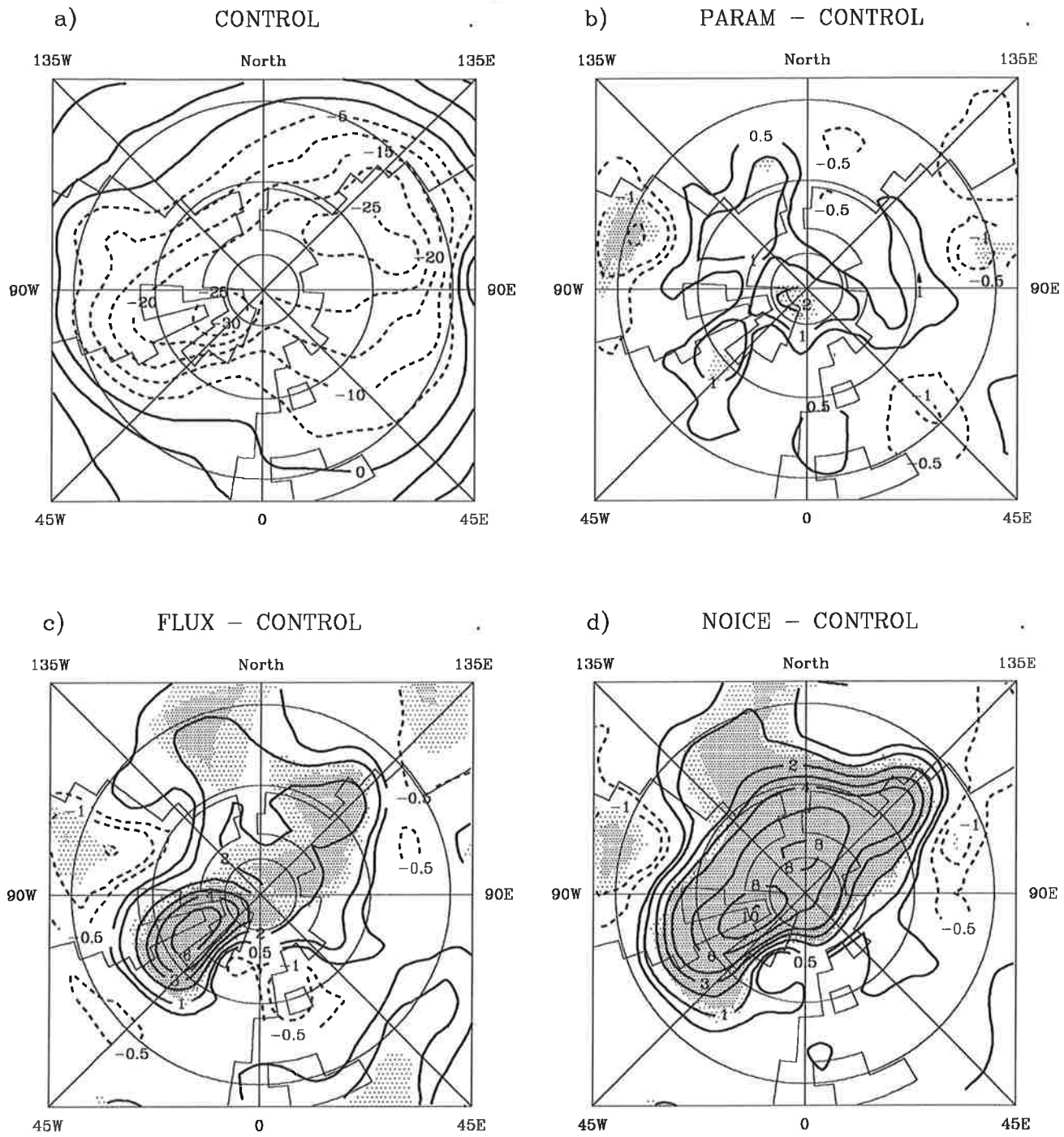

Figure 10: Horizontal distributions of the 850 hPa temperature [°C] for the control experiment (CONTROL) and their changes in the experiments with parameter aggregation (PARAM minus CONTROL), flux-aggregation (FLUX minus CONTROL) and the total removal of the sea ice (NOICE minus CONTROL). The contour interval in Fig. a is 5 °C. In the difference plots contours are shown for ±0.5, ±1, ±2, ±3, ±4, ±6, ±8, ±10 °C. The light and dark shadings show those areas, where the changes are significant at a 95 % and 99 % level, respectively, according to a local t-test.

northerly in all the experiments.

The main features of the experiment with ice supression in the Arctic are comparable to those obtained by Royer et al. (1990), although their maximum warming west of Greenland is with a value of 7 K somewhat lower. In the mid latitudes, the correspondence is not that good, especially over Northern America, the reponse is opposite. But this is not surprising having in mind the high internal variability of the mid latitudes, especially over the continents and their short simulation interval of only 90 days.

As one might expect from the zonal mean temperatures, no important response signals appear in the experiment with parameter aggregation in levels far above, eg. at 500 hPa. In the experiments with flux aggregation or the removal of the sea ice the main features of the 850 hPa temperature changes are still present at 500 hPa. The maxima of the warming are at the same places, only their amplitudes are reduced and have values of approx. 2 K. Also a cooling in the mid latitudes can be observed with amplitudes which are almost the same as those of the corresponding feature at 850 hPa.

5.7 Geopotential height at 500 hPa

The responses of the 500 hPa geopotential height fields (Figure 11) look quite similar to those of the temperature fields. In the experiment with parameter aggregation (PARAM) the response pattern is quite noisy and the statistical significance of the changes is quite low. Thus we will not discuss this experiment further.

The response in the FLUX experiment is much stronger. The tropospheric warming causes a lifting of the pressure levels over the Arctic and the surrounding areas. The main impact in both experiments is found over Greenland and Labrador with an increase in the 500 hpa geopotential height of about 12 gpdm. This pattern is significant at a rather high level. Over the Central Arctic, Alaska and the Northern Pacific a significant increase of 4 gpdm is simulated in the FLUX experiment. Over the Ural mountains changes in the order of 2 gpdm are found, which are not significant. Nevertheless, we think that they should be also attributed to the forcing of the experiment and not to internal variability as we can conclude from the NOICE experiment. In that experiment almost the same pattern appears, but with higher amplitudes and thus with higher statistical significance: changes of 4 gpdm over Alaska, 8 gpdm in the inner Arctic and 6 gpdm over the Ural mountains.

Outside the warming areas in the mid-latitudes, regions of reduced geopotential height are simulated. Over the Atlantic a decrease of up to 2 gpdm, over the Eastern Pacific of 4 gpdm is found in both experiments (FLUX and NOICE). This is the only impact outside the Arctic with a reasonable statistical significance. Over America a reduction of 1 gpdm in the FLUX

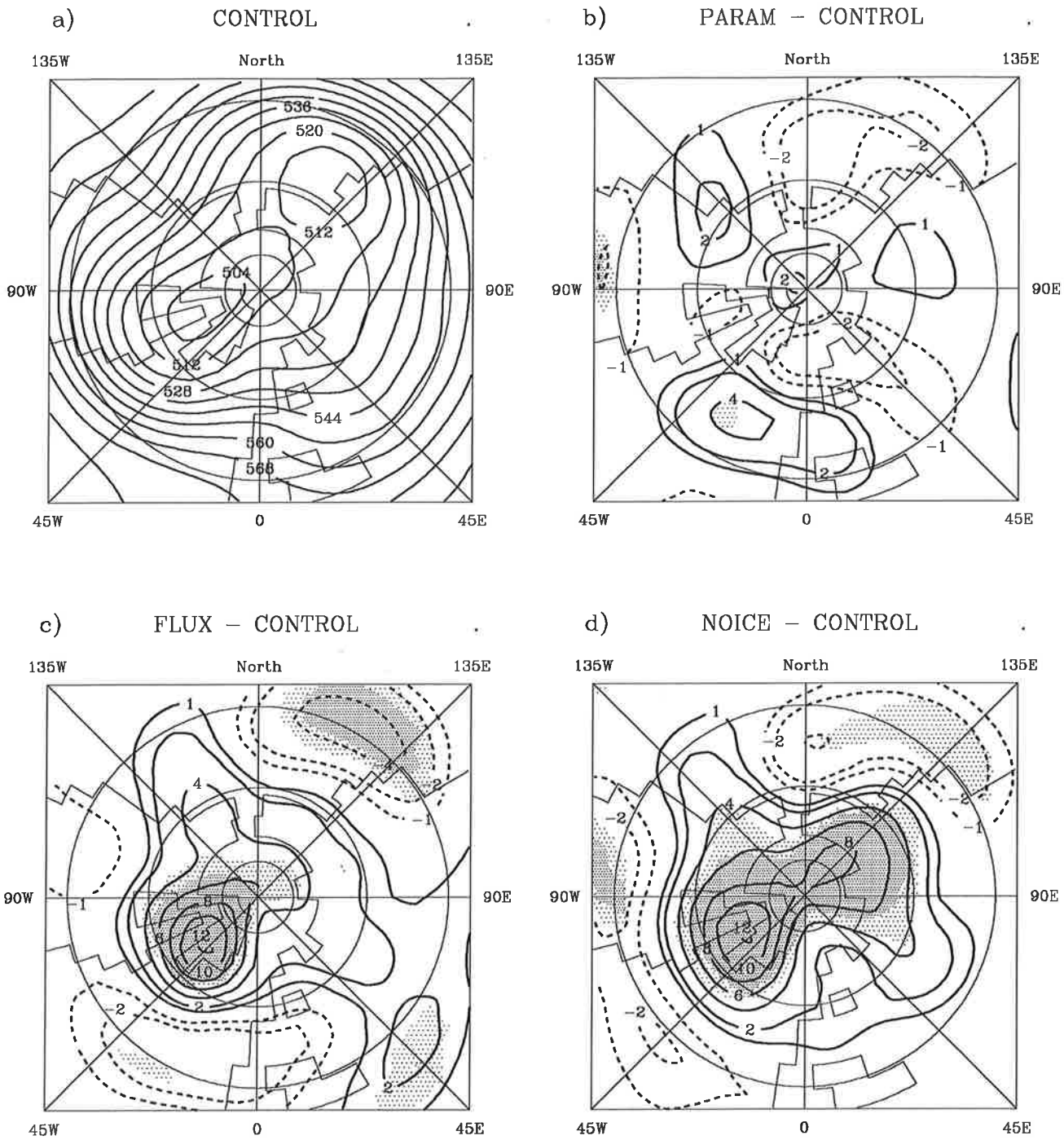

Figure 11: Horizontal distributions of the 500 hPa geopotential height [gpdm] for the control experiment (CONTROL) and their changes in the experiments with parameter aggregation (PARAM minus CONTROL), flux aggregation (FLUX minus CONTROL) and the total removal of the sea ice (NOICE minus CONTROL). The contour interval in Fig. a is 8 gpdm. In the difference plots contours are shown for ±1, ±2, ±3, ±4, ±6, ±8, ±10, ±12 gpdm. The light and dark shadings show those areas, where the changes are significant at a 95 % and 99 % level, respectively, according to a local t-test.

experiment and 2 gpdm in the NOICE experiment is simulated.

The most important feature in the response of the geopotential height fields is the weakening of the Northern American trough in the Greenland and Labrador areas. This is also the main forcing region in both the NOICE and the FLUX experiments. The weakening of that trough might have strong impacts on the climate of the Northern Atlantic. In the Pacific sector the forcing due to the reduction of the sea-ice cover is much weaker and the warming of the troposhere is more limited. Thus, only the northern edge of the Pacific trough is slightly reduced. More to the south, the Pacific trough is remarkably enhanced in both experiments. This is surprising, because it cannot be explained by direct warming caused by the local impact of the sea-ice modifications. There are hints that the intensification of the Pacific trough might be a remote effect caused by the impacts in the Atlantic sector.

The ECHAM model exhibits a strong teleconnection between the Northern American and the Pacific trough. Figure 12 shows a one-point correlation map of the 500-hPa geopotential height calculated from results of the control run on a monthly mean data basis. The temporal correlation of geopotential height at a model grid point located over Greenland, where the maximum impact in sensitivity experiments was found, with all other grid points was calculated. A strong anti-correlation of more than -0.6 between the two Northern Hemispheric troughs can clearly be identified. Their anti-correlation is caused by internal variability of the model. We suppose that this internal mode might be stimulated in the FLUX and NOICE experiments by the weakening of the Northern American trough resulting in an intensification of the Norhern Pacific trough.

5.8 Sea Level Pressure

From purely thermodynamical considerations, a decrease of sea level pressure should be the consequence of the tropospheric warming in the Arctic (Figure 13). This feature is found in the NOICE experiment, where a pressure decrease of 4 hPa is simulated over the central Arctic. Nevertheless, this expected feature is not that sure because of the variability of the data in that region. In the FLUX experiment such a pressure decrease is totally absent.

Very pronounced in both experiments is the weakenig of the Islandic low by approximately 10 hPa. This pressure increase can only be caused dynamically, because it is located in the region with maximum warming as it was shown before. The increase of sea level pressure extends over the Northern Atlantic and Europe in both experiments (FLUX and NOICE). In the FLUX experiment the pressure increase extends westwards over Canada with maximum changes of 4 hPa. In the NOICE experiment another significant maximum of pressure increase is found over Siberia. The intensification of the Northern Pacific trough, as it was discussed before at the geopotential height fields, is also apparent in the pressure maps for

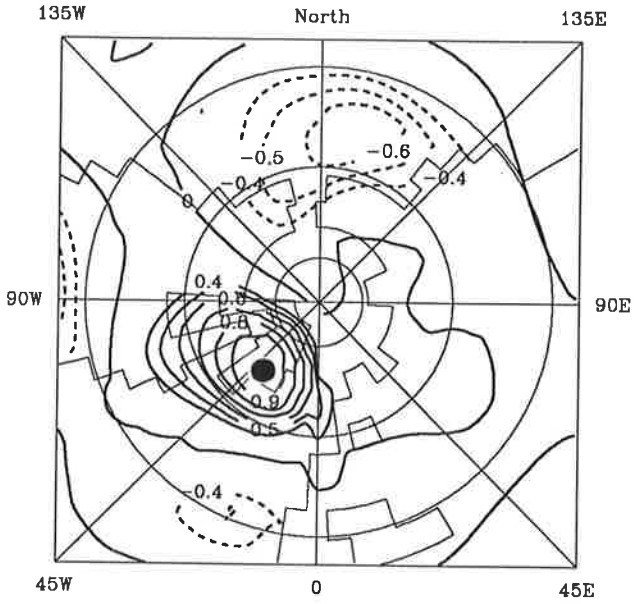

Figure 12: One-point correlation map of the 500-hPa geopotential height for the control experiment. The height at the marked grid-point ● has been correlated with all other grid-points.

both experiments. The Aleutian low is intesified significantly. In the flux averaging experiment the sea level pressure decreased over a large area of the Northern Pacific by more than 4 hPa. In the NOICE experiment the pressure also decreases over such a large area, but with two separate maxima of change over the Bering Sea and over the Sea of Ochotosk (8 hPa and 4 hPa). The intesification of the Aleutian low is caused dynamically, as it was explained before. Nevertheless, the extreme pressure decrease over the Bering Sea in the NOICE experiment might be also induced thermodynamically due to the intensive warming after the removal of the ice in that region. Another area of pressure decrease (~ 2 hPa) appears in both experiments over the mid-latitude Atlantic. Nevertheless, the statistical significance of that feature is quite low.

The most important impact of the sea-ice reduction to the Northern Hemispheric circulation both in the FLUX and the NOICE experiment is the weakening of the Northern American trough and of the Islandic low. The cause seems to be a modified behaviour in the transient variability in the sensitivity experiments. The greatest influences of the sea-ice modifications on the thermal structure of the atmosphere are located in the area of the Hudson Bay, Labrador and the Norwegian Sea. Especially the horizontal temperature gradient in the area of cyclogenesis in the Western Atlantic is essentially reduced. A reduced cyclonic activity should be the consequence of the decreased baroclonicity. Since the quasistationary Islandic low is maintained by the transient activity in the Northern Atlantic, a weakening of the

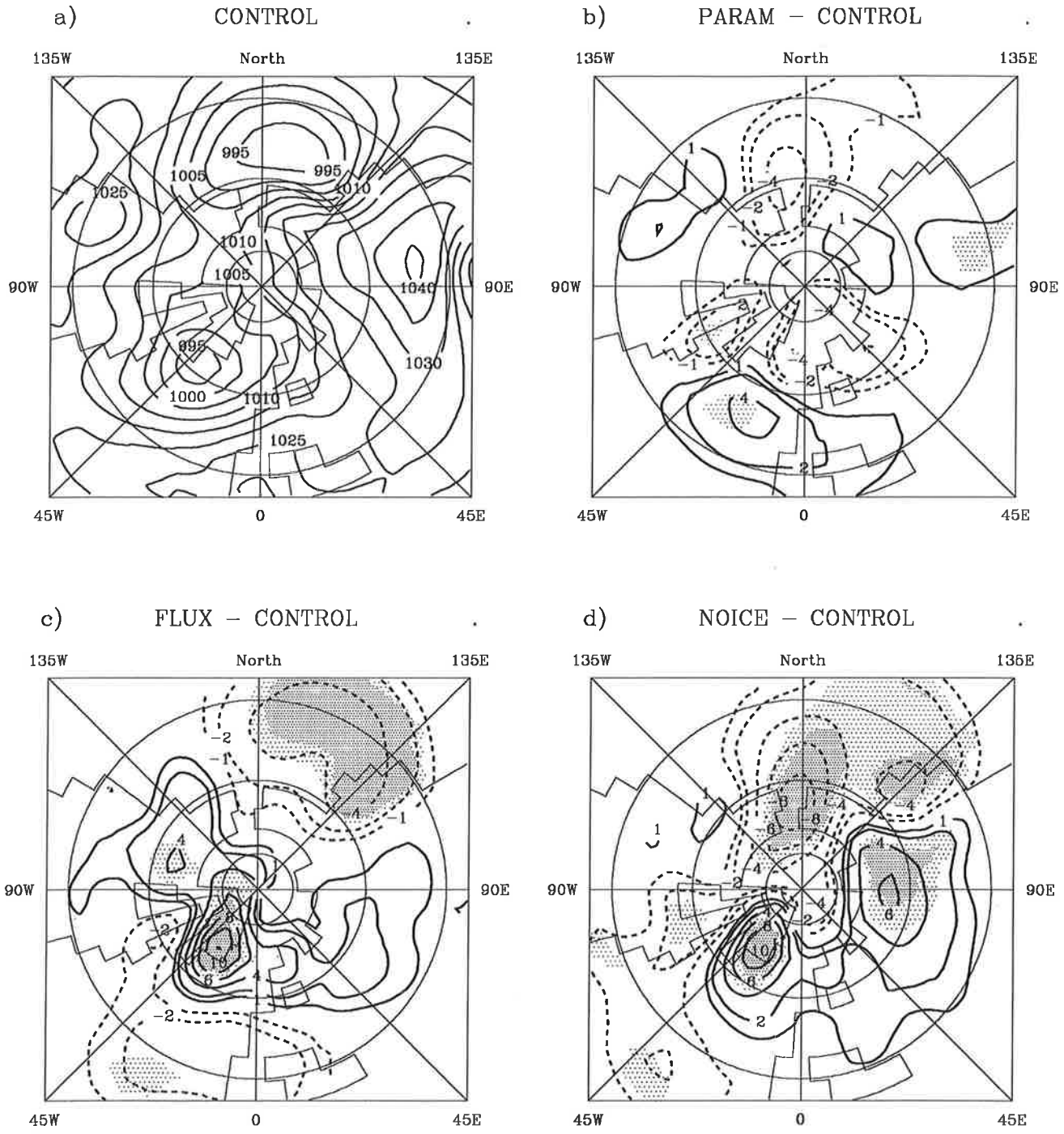

Figure 13: Horizontal distributions of the sea-level pressure [hPa] for the control experiment (CONTROL) and their changes in the experiments with parameter aggregation (PARAM minus CONTROL), flux aggregation (FLUX minus CONTROL) and the total removal of the sea ice (NOICE minus CONTROL). The contour interval in Fig. a is 5 hPa. In the difference plots contours are shown for ±1, ±2, ±3, ±4, ±6, ±8, ±10, ±12 hPa. The light and dark shadings show those areas, where the changes are significant at a 95 % and 99 % level, respectively, according to a local t-test.

Islandic low in the sensitivity experiments seems to be quite reasonable. Nevertheless, these connections are difficult to detect in the simulation results. The transient variability and the cyclonic activity are highly variable themselves even on a monthly mean data basis. The response patterns are very noisy and statistical significant signals can hardly be identified. The results show in the FLUX and the NOICE experiment some reduction of the cyclonic activity over the Northern Atlantic with the strongest reduction southeast of Greenland what is quite consistent with our hypothesis. Also in the northern part of the Western Pacific a slight reduction of cyclonic activity can be observed. But the results also show an intensification southwards of these regions indicating that there could be a southward shift of the stormtracks. In the PARAM experiment almost no impact related to the modified sea-ice distribution can be detected. Nevertheless, these results cannot be viewed to be reliable due to the lack of statistical significance. Even 21 months of January simulation are not enough for a detailed analysis of the impacts of the sea-ice modifications to the transient behaviour of the ECHAM model.

5.9 Baroclinicity

Some evidence for a reduction of cyclonic activity can be obtained from an analysis of the baroclonicity in the Northern Hemisphere stormtrack region. For this purpose, we calculated the baroclonicity for the different experiments following Hoskins and Valdez (1990). The baroclonicity σ_{BI} , which is defined as the growth rate of the first baroclinic mode in the "Eady-model", is given by :

$$\sigma_{BI} = 0.31 f \left| \frac{\partial \vec{v}_G}{\partial z} \right| N^{-1}$$

where f denotes the Coriolis parameter. The vertical gradient of the geostrophic wind $\frac{\partial \vec{v}_G}{\partial z}$ is a measure for the horizontal temperature gradient while the vertical stratification is expressed by the Brunt-Väisälä frequency N. The baroclonicity should be calculated in the lower troposphere just above the boundary layer. Figure 14 shows the baroclonicity for the different experiments taken between the 850 hPa and the 700 hPa level.

For the control run (CONTROL) the areas of cyclogenesis are clearly to identify in the Western Atlantic and the Western Pacific with growth rates of 0.8 and 1.0 per day, respectively. As expected from the temperature response no clear impact on the baroclinicity is found in the experiment with parameter aggregation. Significant reductions of the baroclinicity are simulated in the FLUX and the NOICE experiments around the whole Arctic ocean reflecting the warming inside that area. Especially, over the Western Atlantic Ocean and the Sea of Ochotosk, the regions of cyclogenesis, reductions of the baroclinicity up to 0.12 per day are visible. In the Western Pacific, southwards of the region of decrease, a

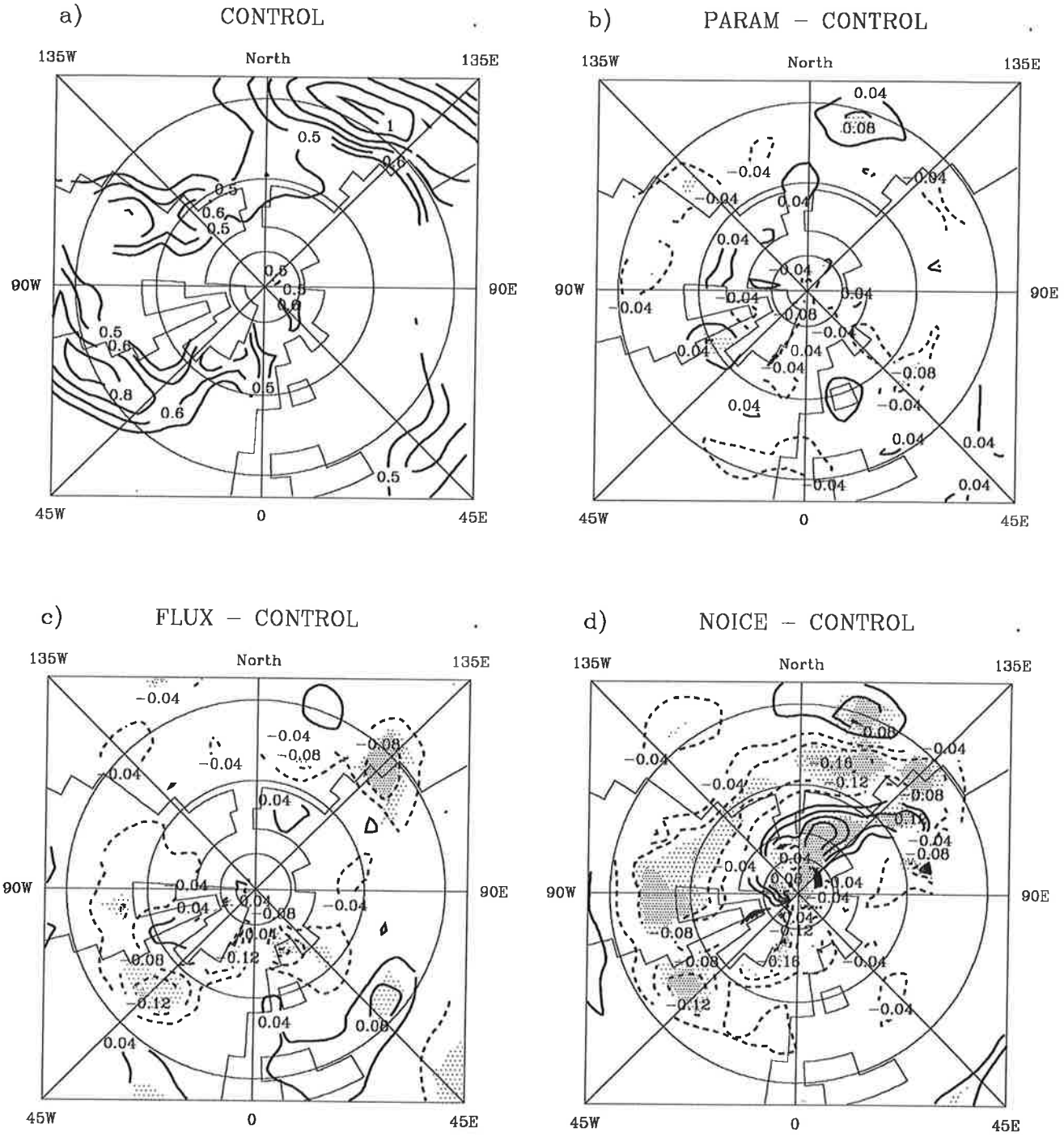

Figure 14: Horizontal distributions of baroclinicity [1/d] at 780 hPa for the control experiment (CONTROL) and their changes in the experiments with parameter aggregation (PARAM minus CONTROL), flux aggregation (FLUX minus CONTROL) and the total removal of the sea ice (NOICE minus CONTROL). The contour interval in Fig. a is 0.1 1/d. In the difference plots contours are shown for ±0.04, ±0.08, ±0.12, ±0.16 1/d. Areas, where the 850-hPa level lies below the earth's surface, have been omitted. The light and dark shadings show those areas, where the changes are significant at a 95 % and 99 % level, respectively, according to a local t-test.

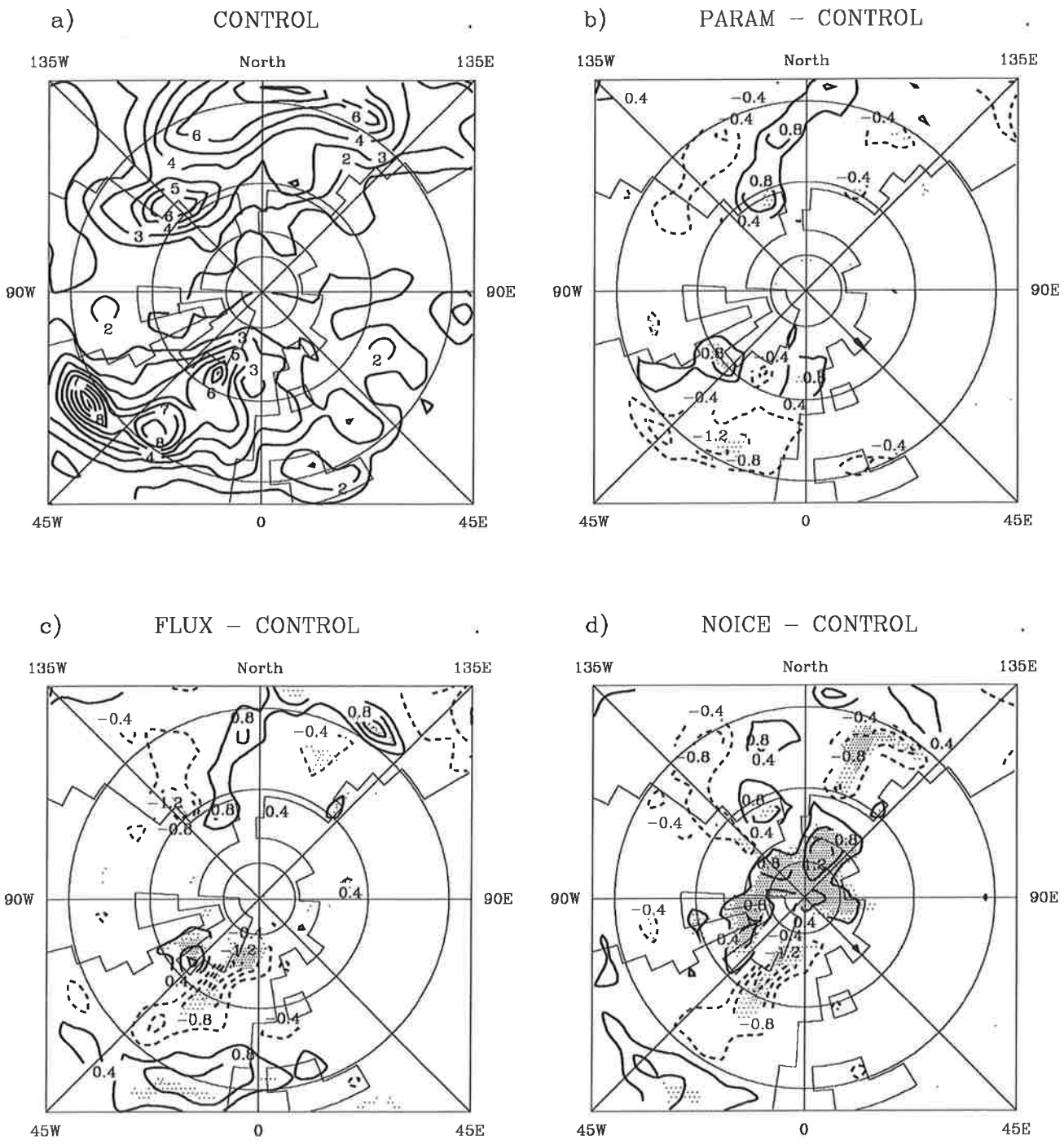

Figure 15: Horizontal distributions of the total precipitation [mm/d] for the control experiment (CONTROL) and their changes in the experiments with parameter aggregation (PARAM minus CONTROL), flux aggregation (FLUX minus CONTROL) and the total removal of the sea ice (NOICE minus CONTROL). The contour interval in Fig. a is 1 mm/d. In the difference plots contours are shown for ±0.4, ±0.8, ±1.2 ±1.6 mm/d. The light and dark shadings show those areas, where the changes are significant at a 95 % and 99 % level, respectively, according to a local t-test.

slight increase of the baroclinicity, especially in the NOICE experiment can be identified. This intensification is connected with the stronger advection of cold air from the Asian continent caused by the intensification of the Northern Pacific trough. In the NOICE experiment another zone of intensified baroclinicity can be seen in the inner Arctic. Due to the removal of the ice cap, the air over the Arctic ocean is now much warmer than that over the surrounding continents leading to a reversal of the meridional temperature gradient. Nevertheless, this region is not important for influences on the cyclonic activity. The strong reduction of the baroclinicity southwest of Greenland and the hints in the analysis of the transient activity support the hypothesis that the weakening of the Islandic low might be caused by a reduction of cyclonic activity in the Northern Atlantic. The connection between sea-ice distribution and cyclonic activity is an interesting question and should be analyzed in more detail. But in order to get reliable results longer integrations under consideration of the seasonal cycle would be necessary.

The reduced cyclonic activity is also apparent in the distribution of the total precipitation (Figure 15). Both the NOICE and the FLUX experiment show a reduction of almost 1 mm/d in the region of the Northern Atlantic stormtrack southwest of Greenland, which is consistent with the response pattern in the cyclonic activity. Also in the region of the Northern Pacific stormtrack, the reduction of cyclones is visible in a significant reduction of precipitation in the Sea of Ochotosk by 0.5 mm/d, especially in the NOICE experiment.

Although the enhanced moisture supply through the leads is connected with an increase in cloudiness in the Arctic in the sensitivity experiments FLUX and PARAM, no important modifications of the precipitation rate are found in that region. However, the precipitation rate in that region is rather small anyway. Only in the experiment with total removal of the sea ice the precipitation is enhanced significantly. In some areas of the Arctic the precipitation rate rised from 1 mm/d to 2 mm/d. Outside the stormtrack regions and the Artic itself hardly any impact on the distribution of the precipitation can be identified in the simulation results.

6. Summary and conclusions

A sub-grid scale sea-ice distribution has been introduced into the Hamburg atmospheric general circulation model ECHAM. Each model grid-box has been divided into an ice-covered and an ice-free part according to a prescribed sea-ice cover. The model, however, requires effective turbulent and radiative fluxes representative for the whole grid-box. Basically, two alternative methods for parameterization are available: A first approach, which has been applied up to now in some coupled ocean-atmosphere models, is to use effective

surface parameters (e.g. an effective surface temperature) obtained by weighted averaging of the local surface properties. A second, more physically based method calculates the fluxes over sea ice and open water separately according to the individual structure of each surface type. Weighted averages of these local fluxes are assumed to be valid for the whole grid-box.

Several sensitivity experiments have been performed in order to study the impact of a sub-grid scale sea-ice cover and the method of parameterization to the surface fluxes and the model climate. The consideration of fractional sea-ice results in a significant modification of the fluxes of sensible and latent heat, and the thermal radiation. In the case of averaging the fluxes (FLUX) this happens even in the inner Arctic, where the fraction of leads is rather small. The impact on the momentum transfer in sea-ice covered regions is quite small. The additional heat transfer in the case of averaging the fluxes warms the lower Arctic troposphere. The warming is spread out into the adjacent areas by advection and horizontal diffusion. The modified Arctic heat budget leads to a significant weakening of the Northern American trough and the Islandic low, while the Northern Pacific trough and the Aleutian low are intensified. The baroclinicity and the cyclonic activity in the Northern Atlantic are reduced. The cloud cover in the Arctic region is enhanced, but no relevant enhancement of precipitation is connected with that. Only in the regions of modified cyclonic activity, a significant reduction of the precipitation is simulated.

These results can only be achieved, if the explicit averaging of the surface fluxes is applied. In some aspects the influence of fractional sea ice is almost in the same order of magnitude than that of a total removal of sea ice. On the other hand, simple averaging of the surface parameters results only in minor impacts on the surface fluxes and the state of the polar atmosphere. Our results clearly show, that the calculation of effective parameters by simply averaging of local parameters is quite problematic. Averaging of the fluxes themselves is the more suitable method, because it takes into account the non-linear dependency of the surface fluxes on the mean flow. Thus we recommend to include fractional sea-ice cover by means of the flux aggregation parameterization in future numerical experiments.

In the current paper we have studied the influence of the sea-ice distribution on the climate of a pure atmosphere model. We expect that the new surface flux parameterization for sea-ice covered areas will have a great influence on the performance of coupled ocean-atmosphere models.

The distribution of sea ice is not the only property of the earths surface which cannot be resolved properly by global circulation models. The snow cover, the land-sea distribution, the distribution of dry and wet soils or the coverage of the earths surface with plants are examples for surface properties, which also have a sub-grid scale distribution. Since the consideration of a sub-grid scale sea-ice cover reveals such strong effects, it could be

speculated that also the sub-grid scale distribution of these other components could be important for the model climate. Thus the method of flux aggregation will be extended to a variety of ground components, and the impact on the model climate will be studied in further numerical experiments.

Acknowledgements: The study was supported by the Deutsche Forschungsgemeinschaft (SFB 318). The simulations have been carried out at the Deutsches Klimarechenzentrum. The authors would like to thank the colleagues of the Meteorologisches Institut der Universität Hamburg, the Max-Planck-Institut für Meteorologie, the Deutsche Gesellschaft für Luft und Raumfahrt and the Deutsches Klimarechenzentrum for their support and helpful discussions.

7. References

Arya, S.P.S., 1975: A drag partition theory for determining the large-scale roughness parameter and windstress on the Arctic pack ice. J. Geophys. Res. **80**, 3447-3454.

Alexander R.C., R.L. Mobley, 1976: Monthly average sea-surface temperatures and ice-pack limits on a global grid. *Mon. Wea. Rev.* **104**, 143-148.

Charnock, M., 1955: Wind stress on a water surface. *Quart. J. R. Meteor. Soc.* **81,** 639-640.

Claussen, M. 1991a: Estimation of areally-averaged surface fluxes, *Boundary-Layer Meteorol.* **54**, 387-410.

Claussen, M. 1991b: Local advection processes in the surface layer of the marginal ice zone, *Boundary-Layer Meteorol.* **54,** 1-27.

Claussen, M., M., Esch, 1993: Biomes computed from simulated climatologies. *Clim. Dyn.* **9**, 235-243.

Claussen. M., 1994a: Estimation of regional heat and momentum fluxes in homogeneous terrain with bluff roughness elements. *Journal of Hydrology,* in press.

Claussen. M., 1994b: Flux aggragation at large scales: On the limits of validity of the concept of blending height. *Journal of Hydrology,* in press.

Cubasch, U., K. Hasselmann, H. Höck, E. Maier-Reimer, U. Mikolajewicz, B.D. Santer and R. Sausen, 1992: Time-dependent greenhouse warming computations with a coupled ocean-atmosphere model. *Climate Dynamics* **8**, 55-69.

ECMWF, 1991: ECMWF forecast model: Physical parameterization. Research manual 3, p. 7.1. Available at ECMWF, Reading, UK.

Gates, W.L., 1992: AMIP: The atmospheric modelling intercomparison project. *Bull. Amer. Meteor. Soc.* **73**, 1962-1970.

Graf, H.F., I. Kirchner, R. Robock and I. Schult, 1993: Pinatubo eruption winter climate effects: Model versus observations. *Clim. Dyn.* **9,** 81-93.

Hibler, W.D., III, 1986: Ice dynamics. In N. Untersteiner (ed.) : The Geophysics of Sea Ice,

Proc. Nato Advanced Study Institute on Air-Sea Inreaction, Plenum Press, NY, pp. 577-640

Hoskins, B.J. and P.J. Valdez, 1990: On the existence of storm tracks. *J. Atmos. Sci.* **47,** 1854-1864.

König, W., R. Sausen and F. Sielmann, 1993: Objective identification of cyclones in GCM simulations. *J. Climate* **6**, 2217-2231.

Ledley, T.S., 1988: A coupled energy balance climate-sea ice model: Impact of sea ice and leads on climate. *J. Geophys. Res.* **93**, 15919-15932.

Lunkeit, F., 1993: Simulation der interannualen Variabilität mit einem globalen gekoppelten Atmosphäre-Ozean Modell. Berichte aus dem Zentrum für Meeres- und Klimaforschung, Reihe A, Nr. 8, Meteorologisches Institut der Universität Hamburg, 142 S, ISSN 0936-949X.

Lunkeit, F., R. Sausen and J.M. Oberhuber, 1994: Climate simulations with the global coupled atmosphere-ocean model ECHAM2/OPYC. Part I: Present-day climate and ENSO events. Max-Planck-Institut für Meteorologie, Hamburg, Report No. 132, 47 pp., ISSN 0937-1060.

Maier-Reimer, E., U. Mikolajewicz, K. Hasselmann, 1993: Mean circulation of the Ham burg LSG OGCM and its sensitivity to the thermohaline surface forcing. *J. Phys. Oceanogr.* **23**, 731-757.

Manabe, S., M.J. Spelman, R.J. Stouffer, 1992: Transient responses of a coupled ocean-atmosphere model to gradual changes of CO_2. Part II: seasonal response. *J. Clim.* **5**, 105-126.

Martin, T., 1993: Multispektrale Meereisklassifikation mit passiven Satellitenradiometern. Berichte aus dem Zentrum für Meeres- und Klimaforschung, Reihe A, Nr. 7, Meteorologisches Institut der Universität Hamburg, 110 S., ISSN 0936-949X.

Mason, P.J., 1988: The formation of areally averaged roughness lengths. *Quart. J.R. Meteorol. Soc.* **114,** 399-420.

Maykut. G.A., 1978: Energy exchange and ice production in the Central Arctic. *J. Geophys. Res.* **83**, 3646-3658.

Meehl, G.A., Washington, W.M., 1990: CO_2 climate sensitivity and snow-ice albedo parameterization in an atmospheric GCM coupled to a mixed-layer ocean model. *Clim. Change* **6**, 283-306.

Meleshko, V.P., B.E. Shneerov, A.P. Sokolov and V.M. Katsov, V.M., 1990: Sea-ice anomaly impact on surface heat fluxes and atmospheric circulation as evaluated by the MGO GCM. Workshop on Polar Radiation Fluxes and Sea-Ice, Bremerhaven, 5-8 Nov. 1990.

Nakamura, N. and A.H. Oort, 1988: Atmospheric heat budget of the polar regions. *J. Geophys. Res.* **93**, 9510-9524.

Newson, R.L., 1973: Response of a general circulation model of the atmosphere to removal of the arctic ice-cap. *Nature* **241**, 39-40.

Noilhan, J. and P. Lacarrère, 1992: GCM gridscale evaporation from mesoscale modelling.

in: Proceedings of a workshop held at ECMWF on fine-scale modelling and the development of parameterization schemes. 16-18.9.1991. 245-274.

Oberhuber, J.M., 1993: Simulation of the Atlantic circulation with a coupled sea-ice mixed layer isopycnal general circulation model. Part I: Model description. *J. Phys. Oceanogr.* ***23***,808-829.

Ponater, M., König, W., R. Sausen and F. Sielmann, 1994: Circulation regime fluctuations and their effect on intraseasonal variability in the ECHAM climate model. *Tellus* **46A**, 265-285.

Roeckner, E., K. Arpe, L. Bengtsson, S. Brinkop, L. Dümenil, M. Esch, E. Kirk, F. Lunkeit, M. Ponater, B. Rockel, R. Sausen, U. Schlese, S. Schubert and M. Windelband, 1992: Simulation of the present-day climate with the ECHAM model: Impact of model physics and resolution. Max-Planck-Institut für Meteorologie, Hamburg, Report No. 93, 171 pp.

Royer J.F., S. Platon and M. Deque, 1990: A sensitivity experiment for the removal of Arctic sea-ice with the French spectral general circulation model, *Climate Dynamics* **5,** 1-17.

Schlesinger, M.E. and J.F.B. Mitchell, 1985: Model projections of the equilibrium climatic response to increased carbon dioxide. In M.c. MacCracken and F.M. Luther (ed.): Projecting the Climatic Effects of Increasing Carbon Dioxide, Rep. DOE/ER-02037, U.S. Department of Energy, Washington D.C., pp. 381.

Simmonds, I., W.F. Budd, 1991: Sensitivity of the southern hemisphere circulation to leads in the Antarctic pack ice. *Q.J.R. Meteorol. Soc.* **117,** 1003-1024.

Smith, S.D., R.D. Muench and C.H. Pease, 1990: Polynyas and Leads: An overview of physical processes and environment. *J. Geophys. Res.* **95**, 9461-9479.

Stössel, A. and M. Claußen, 1993: On the momentum forcing of a large-scale sea-ice mo del. *Climate Dynamics* **9**, 71-80.

Washington, W.M., A.J. Sempter, C. Parkinson and L. Morrison, 1976: On the development of a seasonal change sea-ice model. *J. Phys. Oceanogr.* **6**, 679-685.

Wieringa, J., 1986: Roughness dependent geographical interpolation of surface wind speed averages. *Quart. J.R. Meteorol. Soc.* **112**, 867-889.

Wood, N. and P.J. Mason, 1991: The influence of stability on effective roughness lenghts for momentum and heat transfer. *Q.J.R. Meteorol. Soc.* **117**, 1025-1056.